C-terminal tagging impairs AGO2 function

Kunal M. Shah*[1], Alex F. F. Crozier*[1], Anika Assaraf[1], Muzjda Arya[1], Paul Grevitt[1], Faraz Mardakheh[1], Michael J. Plevin[3] and *Tyson V. Sharp*[#1]

1. Centre for Cancer Cell and Molecular Biology, Barts Cancer Institute, Queen Mary University of London, John Vane Science Centre, Charterhouse Square, London EC1M 6BQ.

2. Centre for Cancer Genomics and Computational Biology, Barts Cancer Institute, Queen Mary University of London, John Vane Science Centre, Charterhouse Square, London EC1M 6BQ.

3. York Structural Biology Laboratory, York Biomedical Research Institute, Department of Biology, University of York, York YO10 5DD, UK.

* These authors contributed equally
# Corresponding Authors:

Abstract

A full understanding of RNA silencing requires appropriate molecular biology tools to explore the roles of Argonaute 2 (AGO2) and the RNA-induced silencing complex (RISC). Approaches relying on affinity tagging and antibodies have important limitations that can lead to artificial results. Both the N- and C-terminal domains of AGO2 have been shown to be important for correct activity and yet the consequences of appending tags to either terminus have not been fully investigated. N-terminal tags are frequently used to study AGO2 biology. Recently, an N-terminal *HaloTag-Ago2* fusion was reported and examined in mice. While the versatile HaloTag provided new opportunities to study RISC biology, the tagged construct showed certain activity changes compared to unmodified AGO2. CRISPaint, a new CRISPR-Cas9 technique, permits the creation of endogenous C-terminal tag fusions. We used CRISPaint to generate the first reported recombinant AGO2 construct with a C-terminal tag: an endogenous C-terminal HaloTag fusion to AGO2 ($AGO2^{HALO}$) in human (A549) cells. We found that the $AGO2^{HALO}$ fusion protein has a reduced capacity to interac with the key protein binding partner TNRC6A and that the C-terminal HaloTag does not affect cell viability. However, the $AGO2^{HALO}$ fusion significantly impairs RNA cleavage and RNA silencing activity compared to control cells and reduces nuclear localisation of the fusion protein. Using plasmid constructs and transient transfection, we compared AGO2 tagged with EGFP at the N- or C-terminus in siRNA and miRNA reporter gene assays, and cellular localisation. N-terminally tagged AGO2 functioned and localised similarly to WT untagged AGO2, whereas C-terminally tagged AGO2 was impaired in siRNA and miRNA silencing and exhibited poor nuclear and P-body localisation. We conclude that the fusion of a C-terminal HaloTag to AGO2 is not appropriate for studying AGO2 and RISC. Our results assert the importance of comprehensively validating recombinant tagging strategies to ensure that any experimental results generated do not arise from, or are not obscured by, critical functional defects.

44 **Introduction**

45 The four human Argonaute proteins (AGO1-4) are key components of the microRNA-induced silencing
46 complex (miRISC), which is critical for the correct regulation of gene expression through miRNA-
47 mediated silencing.[1,2,3,4,5,6,7] Due to the considerable scientific and clinical interest in RNA silencing,
48 exemplified by the recent Nobel Prizes to Ambrose and Ruvkun, a significant body of work has been
49 performed to develop experimental tools for the study of AGO protein function. However, assay
50 design has been limited by methods that rely on antibodies and affinity/auto fluorescent tags, which
51 can be technically challenging and often lack the sensitivity or specificity required to generate
52 appropriately robust results.

53 Recombinantly tagging a protein of interest is a widely used strategy in molecular biology and
54 biotechnology to purify, visualise, and manipulate target proteins. To overcome challenges related to
55 antibody specificity and pull-down efficiency attempts to study RISC have often used overexpressed,
56 recombinantly-tagged AGOs. Such approaches, however, carry the risk of generating artefacts. For
57 example, a N-terminal Flag-tagged AGO2 construct resulted in five-fold over-expression compared to
58 endogenous AGO2 levels, altered AGO2 sub-cellular localisation, and resulted in the identification of
59 potentially false binding partners.[8] Such artefacts might arise from either over-expression of the
60 transgene or the presence of the Flag tag itself. Moreover, it has been shown that recombinantly-
61 tagged, over-expressed proteins can non-specifically localise to processing (P) bodies.[10] Caution
62 should therefore be applied to any study that uses recombinantly-tagged proteins to show that both
63 AGO and TNRC6 proteins are strongly localised to P bodies.[0] Consequently, approaches that tag
64 endogenous proteins are often deemed more desirable. However, this too can disrupt normal protein
65 function.[11,12] In rapidly proliferating cell lines, endogenously tagged AGOs have been shown to elute
66 in complexes of more variable size than native AGOs have, which primarily elute as components of
67 high molecular weight complexes.[13,14] An endogenous N-terminal EGFP-AGO2 fusion protein was not
68 recognised by a pS387-AGO2-specific antibody in immunofluorescence assays, conceivably due to the
69 tag altering AGO2 conformation and therefore reducing pS387 antibody binding.[15] Even in cases where

70 endogenous tags have been shown to retain core RISC activity, these tagged proteins should only be
71 used to study known RISC functions under specific experimental conditions and periods of expression.
72 The use of novel tags and tagging strategies in different cell models may affect the target protein to
73 unpredictable extents. Nevertheless, protein tagging can expand our ability to study RNA silencing and
74 RISC proteins, albeit with (manageable) technical biases which are inevitable when probing complex
75 biological systems. Thus, to confidently exploit the potential benefits that recombinant tagging of
76 endogenous proteins offers it is important to ensure that the core functionalities of the proteins of
77 interest are sufficiently retained - primarily through considered design and stringent validation - and
78 that technical biases should be considered and minimised when designing experiments and
79 interpreting results.

80 The HaloTag protein fusion platform is a modular protein tagging system that can be programmed for
81 different functions, proving a versatile technology.[16,17,18] The modified 33 kDa haloalkane
82 dehalogenase HaloTag protein can covalently bind to synthetic chloroalkane ligands (collectively
83 known as HaloTag ligands) which comprise a chloroalkane linker attached to a variety of useful
84 molecules, such as fluorescent dyes, affinity handles, or solid surfaces. Covalent bond formation
85 between the protein tag and the chloroalkane linker is high affinity, rapid, specific, and irreversible.
86 This enables efficient purification of HaloTag fusion proteins and means this single genetic construct
87 can have multiple capabilities to comprehensively analyse protein function and interaction.
88 Importantly, an endogenous fusion of HaloTag to the N-terminus of *Ago2* (HaloTag-Ago2) has enabled
89 the high-resolution identification of Ago2-miRNA and -mRNA interactions in mice.[14]

90 Applying UV crosslinking to cells expressing HaloTag fusion proteins enables efficient identification of
91 RNA targets of RNA-binding proteins.[19] Of note, HaloTag-Ago2 fusions have been used to investigate
92 the association of Ago proteins with RNA in a process termed Halo-Enhanced Ago2 Pulldown
93 sequencing (HEAP-seq).[14] The HaloTag ligand conjugated to a resin can be used to pull down HaloTag-
94 Ago2 in cells or tissues expressing the fusion. High-throughput sequencing of RNA extracted from
95 purified AGO-miRNA-mRNA complexes then enables the identification of miRNA-mRNA networks

96 under physiological (and/or pathological) conditions. In addition to bypassing the need for
97 radiolabelling, immunoprecipitation, and gel purification, the covalent nature of the interaction
98 between the HaloTag and its ligand simplifies the isolation of AGO-miRNA-mRNA complexes, removing
99 the intrinsic variability of antibody-based approaches. Moreover, as the strong covalent bond permits
100 more stringent washing, there is less potential for non-specific RNAs to be captured. [14,20] Accordingly,
101 HEAP-seq was demonstrated to enable both more sensitive and specific identification of AGO protein-
102 RNA interactions than conventional methods which rely on the use of antibodies to precipitate AGO-
103 containing complexes (i.e. CLIP-seq[21]). Furthermore, the HaloTag labelling capacity can also be used
104 to perform live-cell single-molecule imaging to observe dynamic activity and high-resolution
105 investigation of protein-protein interactions through mass spectrometry.[17,22,23,24] Endogenous fusion
106 of AGO2 to HaloTag should therefore facilitate a thorough investigation of AGO2/RISC in human cells
107 at physiologically relevant abundancies, in near-native cellular background, and to greater resolution
108 than antibody-based approaches. Future HaloTag:AGO1-4 fusions would also enable comparative
109 analysis of AGO1-4 biology in different contexts, with the mutual HaloTag overcoming the key
110 limitations of CLIP-based methods that result from variable antibody performance.

111 AGO2 comprises four domains (N-terminal (N), PIWI/Argonaute/Zwille (PAZ), middle (MID), and P-
112 element-induced wimpy testes (PIWI)), each with known roles in RISC formation and RNA
113 silencing.[25,26,27,28,29,30] When designing a recombinantly-tagged AGO2 protein, it is critical to consider
114 the impact on both N- and C-terminal domains. The PIWI domain is located at the C-terminus of AGO2.
115 This domain contains six loops along the nucleic acid-binding cleft and is similar in function to an RNase
116 H domain, harbouring the catalytic tetrad (DEDH) essential for the slicing activity of
117 AGO2.[30,31,32,33,34,35,36,37] Mutation of the conserved glutamate residue in the DEDH motif abolishes the
118 ability of AGO2 to induce RNAi.[36] Many post-translational modifications (PTMs) of AGO2 are found in
119 the C-terminal PIWI domain.[38] These PTMs impact various aspects of AGO2 function, influencing both
120 RISC and miRNA activity. The C-terminal half of human AGO2 is also responsible for the interaction
121 with TNRC6A, which is crucial for miRNA-dependent silencing function and the localization of AGO2 in

122 cytoplasmic foci.[6] The N domain of AGO2 is fundamental to RISC functionality, facilitating ATP-
123 independent unwinding of small RNA duplexes, a critical step for RISC assembly in human cells. Both
124 slicer-dependent and slicer-independent unwinding require efficient function of the N domain of
125 AGO2, highlighting its importance in passenger-strand cleavage. Moreover, two specific motifs
126 (residues 44–48 and 134–166) in the N-terminal region of AGO2 are vital for optimal catalytic activity.
127 It is postulated that, due to their proximity to the PIWI domain in the tertiary structure of AGO2, these
128 motifs are essential for the accurate positioning of the guide:target. Alterations within these motifs
129 hinder the activation of RISC and obstruct mRNA cleavage.[38,39,40] Deletion of the N-terminal, Linker 1
130 and PAZ domains in *Drosophila* AGO2 resulted in decreased target RNA binding and constitutive
131 activation of the cleavage activity of the PIWI domain.[41] These studies highlight the collective
132 importance of both the N- and C-termini in the normal function of AGO2 and emphasise the need for
133 consideration and due diligence when adding and validating tags at either terminus, as each may
134 disrupt normal protein function.

135 We set out to develop human cell lines endogenously expressing AGO2 fused to a reporter tag to
136 enable comprehensive study of AGO2 function and RISC biology in cells relevant to our research
137 interests. Due to the stated versatility of HaloTag technology and advantages over traditional methods
138 used to study AGO complexes and RISC, we sought to generate a AGO2-HaloTag fusion protein. A
139 previous study that used N-terminal fusion of HaloTag with Ago2 reported diminished ability to rescue
140 RNAi in *Ago2*$^{-/-}$ MEFs compared to WT Ago2, de-repression of a subset of highly expressed miRNA
141 targets, and reduced viability of *HaloTag-Ago2* homozygous mice,[14] indicating some loss of
142 functionality due to the N-terminal HaloTag-Ago2 fusion. A series of functional validation experiments
143 did, however, demonstrate core functionalities were retained after N-terminal HaloTag-Ago2 fusion.
144 Pull-down assays established physical interaction between HaloTag-Ago2 and the core miRISC
145 component Tnrc6a, while size-exclusion chromatography showed co-elution of HaloTag-Ago2 with WT
146 Ago2 in high molecular weight complexes (though, notably, complexes were of more variable size in
147 tagged cells[9]). Encouragingly, Dual-Luciferase reporter experiments using three constructs with well-

148 characterized miRNA binding sites, as well as a sensitive two-colour fluorescent reporter system,[42]
149 showed no detectable differences in miRNA-mediated repression between *WT* and *Ago2*$^{Halo/Halo}$ MEFs.
150 These findings are an example of orthodox tag validation and, overall, indicate endogenous N-terminal
151 fusion of HaloTag to AGO(2) is a valuable model to study miRISC *in vivo* and *in vitro*, despite some
152 reported functional limitations. However, the tagging approach used by Li *et al*. raises important
153 points of consideration when designing tags. N terminal fusion of HaloTag to Ago2 was achieved by
154 insertion of a conditional knock-in allele containing the HaloTag upstream of a loxP-STOP-IRES-FLAG-
155 loxP cassette in mouse ES cells to express Cre recombinase which fuses the HaloTag to the first exon
156 of *Ago2*.[14] This is a relatively complex method of gene tagging which can be time-consuming and
157 challenging to precisely reproduce. The approach also disrupts the 5' UTR of the *Ago2* gene, risking
158 unknown effects on the regulation of expression of AGO2, which is critical when considering true *in*
159 *vivo* endogenous functionality. These challenges therefore prompted us to look for alternative
160 methods to generate an endogenous HaloTag fusion to AGO2 in human cells.

161 CRISPaint is a gene editing system which allows the precise creation of C-terminal tag fusions of
162 endogenously encoded proteins in human cells with high efficiency.[43] Unlike homology directed repair
163 (HDR)-directed tagging, CRISPaint does not require generation of a site-specific donor template with
164 homology arms but integrates heterologous genetic material via canonical non-homologous end
165 joining (cNHEJ) in CRISPR-Cas9-accessible cellular systems. This reduces the overall time required to
166 obtain genetically tagged cells compared with HDR-directed tagging.

167 The lack of data on the validity of C-terminal AGO2 tagging, the non-trivial nature of endogenous N-
168 terminal AGO2 tagging using the method used by Li *et al*, the importance of the 5' UTR, and the critical
169 motifs at both the C- and N-termini of AGO2 together make a preferred strategy for generating tagged
170 variants of endogenous AGO2 tags challenging to predict. We therefore employed CRISPaint to create
171 cell lines expressing a C-terminal AGO2-HaloTag fusion protein (AGO2^{HALO}) for the future
172 comprehensive study of AGO2 in human cells. Due to the addition of the tag potentially impairing
173 normal protein function and therefore invalidating any future results, as well as the lack of published

174 evidence on the effect of C-terminal tagging of AGO2, we sought to validate the functional activity of
175 endogenous AGO2^{HALO} robustly and diligently against native AGO2 in UnTagged CRISPaint controls
176 lines and *WT* A549 cells.

177

178 By interrogating the core functional activities of AGO2 (protein localisation and binding, cleavage, and
179 silencing capacity) in *WT*, UnTagged, and *AGO2^{HALO}* cells, we aimed to define the impact of the C-
180 terminal fusion of AGO2 with HaloTag. Our results led us to conclude that *AGO2^{HALO}* cells have
181 significantly impaired silencing function compared to control UnTagged and *WT* AGO2 cells, as well as
182 distinct sub-cellular localisation. We therefore do not consider C-terminal AGO2^{HALO} as a suitable
183 model for further study of AGO2 and RISC function. Although we only considered a single configuration
184 for a single type of C-terminal fusion tag of the relatively large (33 kDa) HaloTag to AGO2, comparison
185 of our data with previously published N-terminal HaloTag-AGO2 does indicate that N-terminal tagging
186 is favourable. Following this, we directly compared the effect of N- vs C-terminal tagging on AGO2
187 function. Addition of an EGFP tag to the C-terminus of AGO2 resulted in a loss of silencing function
188 comparable to complete AGO2 ablation, whereas addition of the same tag at the N-terminus had no
189 such effect with silencing function maintained. Together, these data indicate C-terminal tagging of
190 AGO2 severely impairs normal AGO2 function and is less suitable than N-terminal AGO2 tagging
191 approaches for study of AGO2/RISC in human cells.

192

193 ## Materials and Methods

194

195 ***Cell Culture***

196 A549 cells were maintained in DMEM (Sigma, D8437) supplemented with 10% qualified fetal bovine
197 serum (FBS) (Gibco, 10270106), 100 U/mL penicillin, and 100 µg/mL streptomycin (Gibco, 15140122)
198 in a humidified 37 °C incubator and 5% CO_2. Cells were passaged every 3-4 days during the log phase
199 of growth with Trypsin/EDTA solution (Gibco, R001100) following a PBS wash. To seed an exact
200 number of cells, cell suspension concentration was counted using a Countess II™ Automated Cell
201 Counter (Invitrogen). Parental stocks were obtained from ATCC. All cell cultures were regularly tested
202 for mycoplasma. Post editing, isogenic lines (A549 WT, UT C1, $AGO2^{HALO}$ C5 and $AGO2^{HALO}$ C10) were
203 authenticated by STR profiling at 16 STR loci (***Supp Fig. 1***) using PCR-single-locus-technology (Eurofins
204 Genomics).

205 ***CRISPaint Transfection and Puromycin Selection***

206 The CRISPaint gene tagging kit was a gift from Veit Hornung (Addgene kit # 1000000086). To generate
207 a targeting construct for AGO2, we used site-directed mutagenesis to change the gRNA sequence for
208 TUBB to AGO2 gRNA sequence (AACATGTCAAGCAAAGTACA) in the pCas9 mCherry TUBB plasmid. For
209 CRISPaint[43] transfection, A549 cells were plated in a 96 well plate and, per well, 50 ng pCas9 mCherry
210 AGO2, 50 ng pCas9 mCherry Frame +1 and 100ng pCRISPaint HaloTag-Puro donor plasmids were
211 transfected using ViaFect (Promega E498A). Three days post-transfection cells were sub-cultured into
212 media supplemented with puromycin (0.8 µg/mL; Invivogen, ANT-PR-1). After six days of selection,
213 cells were allowed to recover in media without puromycin for 12 days, followed by another round of
214 puromycin selection for six days. After recovery, the cells were grown out in sufficient quantities to
215 perform Western blotting of whole cell lysates of mixed populations. This was followed by single cell
216 cloning in 96 well plates and once grown in sufficient quantities, individual clones were
217 immunoblotted using the anti-HaloTag antibody (Promega) to screen for the AGO2-HaloTag fusion of
218 approximately 130 kDa molecular weight. Two clones with no tagging of AGO2 (**UnTagged *C1*** and
219 **UnTagged *C2***) and two expressing AGO2-HaloTag (**$AGO2^{HALO}$ C5** and **$AGO2^{HALO}$ C10**) were selected for
220 further evaluation in this study, alongside parental ***A549 WT*** cells. A schematic of the experimental
221 design employed to generate and select *AGO2-HaloTag* (and non-transfected (UnTagged)) CRISPaint
222 clones is provided in ***Fig. 1C***.

223 ***Genomic DNA Sequencing at AGO2-HaloTag Junction***

224 Genomic DNA was prepared by removing the media and lysing the cells in 30 µl of gDNA lysis buffer
225 (0.2 mg per mL proteinase K, 1 mM $CaCl_2$, 3 mM $MgCl_2$, 1 mM EDTA, 1% Triton X-100 and 10 mM Tris
226 pH 7.5) and then incubating samples at 65 °C for 10 min and at 95 °C for 15 min. The *AGO2-HaloTag*
227 junction region of this genomic DNA was amplified in a 25 µl Phusion Hot Start Flex (M05365S, NEB)
228 PCR reaction as per the manufacturer's instructions, using specific forward
229 (CAGCTGCTTTTCTGGAAGGG) and reverse (TCTTATGTACCTGACCGACG) primers. Following
230 confirmation of correct PCR amplification on an 0.8% agarose Tris borate EDTA gel, PCR products were
231 TOPO cloned using Zero Blunt™ TOPO™ PCR Cloning Kit for Sequencing (ThermoFisher K287520),
232 transformed into 5-alpha Competent *E. coli* (C2987I, NEB) as per the manufacturer's protocol for
233 plasmid preparation. Transformed colonies (≥ 5) were grown out in LB medium with 50 µg/mL
234 Kanamycin and then pelleted before plasmids were isolated using the Monarch Plasmid Miniprep Kit

235 (NEB, T1010L). Plasmids were sequenced (Sanger) from the T7 priming site of Blunt II-TOPO vector.
236 Sequencing alignment was performed on BioEdit software.

Genomic DNA Primers	Sequence
AGO2 last intron FWD (Blue)	CAGCTGCTTTTCTGGAAGGG
AGO2 last exon REV (Blue)	CGTCTCATGTTCGATGCTGG
HaloTag FWD set 1 (Light Teal)	CCTGATCGGTATGGGCAAAT
HaloTag REV set 1 (Light Teal)	GGGCGGATGAACTCCATAA
HaloTag FWD set 2 (Dark Teal)	ACCAGACCTGGGTTATTTCTTC
HaloTag REV set 2 (Dark Teal)	GCAGCCAGTCCATGTATTCT

237

238 ***AGO2 knockout A549 generation***

239 Using the Horizon Discovery Edit-R CRISPR system, wild type A549 cells were transfected with Cas9
240 nuclease mRNA, TRACrRNA and two crRNAs targeting AGO2 at exon 2 and exon 15 according to
241 manufacturer's instructions. DharmaFECT Duo transfection reagent was used to transfect cells. Four
242 days post-transfection, some cells were collected to extract genomic DNA for T7 endonuclease assay
243 to assess editing efficiency and the rest of the cells were expanded. From the heterogenous cell
244 population, single cell clones were obtained by plating cells at 0.7 cells per well in 96 well plates. Single
245 cell clones were screened for loss of AGO2 expression by immunoblotting using rabbit anti-AGO2 (Sino
246 Biological 101620-T36). AGO2 knockout clones were expanded and frozen in liquid nitrogen.

247 ***Cloning of AGO2 in pEGFP-C1 and pEGFP-N1***

248 AGO2 cDNA was generated from total human RNA from H358M cells using a gene-specific reverse
249 primer and the SuperScriptIII reverse transcriptase (Life Technologies), according to manufacturer's
250 instructions. Using 2X Q5 hot start PCR master mix (NEB), AGO2 cDNA was amplified from the cDNA
251 using forward and reverse primers containing specific restriction enzyme sites for the vectors to be
252 cloned into: for cloning into pEGFP-C1 (to make N-terminally tagged AGO2), HindIII in the forward
253 primer and BamHI in the reverse primer; for cloning into pEGFP-N1 (to make C-terminally tagged
254 AGO2), EcoRI in the forward primer and BamHI in the reverse primer. Following agarose gel
255 electrophoresis to confirm correct size of products, gel extraction was carried out and restriction
256 digestion performed on insert and vector DNA. Ligation was performed using Instant sticky-end ligase
257 mix (NEB) and DH5a E. coli were transformed with ligation reactions. Bacteria were selected on LB
258 agar plates containing kanamycin. Colonies were picked and miniprep cultures were set up.
259 Miniprepped DNA (prepared with Monarch plasmid DNA extraction kit) was sequenced to confirm
260 insertion of AGO2 at the correct sites.

261 To generate a vector expressing WT AGO2 without a tag, pEGFP-C1 AGO2 was digested with NheI-HF
262 and HindIII to excise the EGFP cassette. This digestion was run on an agarose gel and the band for the
263 remaining vector was excised and gel extracted. Sticky ends were blunted with blunt enzyme mix
264 (NEB) and the vector was recirularised using Quick ligase. Following bacterial transformation and
265 selection on LB agar plates containing kanamycin, miniprep cultures were set up and plasmid DNA was
266 extracted and sequenced.

267 ***Analysis of Cell Doubling Time***

268 Cell doubling time was measured using the IncuCyte ZOOM live-cell imaging platform (Essen
269 Bioscience). Cells imaged using the IncuCyte were seeded in triplicate into 24 well plates at 12,000

270 cells per well and imaged at 10x magnification every 12 hours for 108 hours. Cell confluence per well
271 was calculated using the IncuCyte ZOOM software (Essen Bioscience). Data represent mean ± SEM of
272 three independent experimental repeats.

273 ***Western Blotting Analysis and Densitometry***

274 Cells were lysed in RIPA buffer (150 nM NaCl, 1% (v/v) IGEPAL, 0.5% (w/v) deoxycholic acid, 0.1% (w/v)
275 SDS, 50 mM Tris) supplemented with protease and phosphatase inhibitors (Pierce, Roche) during the
276 log phase of growth. Protein concentration was quantified using the Pierce BCA protein assay kit
277 (ThermoFisher Scientific, 23225). Lysates were electrophoresed on polyacrylamide gels transferred
278 onto PVDF membranes and probed using the following antibodies: mouse anti-beta-Actin (Sigma
279 #A1978), mouse anti-Vinculin (Invitrogen, 14-9777-82), rabbit anti-AGO1 (CST, 5053), rabbit anti-
280 AGO2 (CST, 2897), rabbit anti-AGO2 (Sino Biological 101620-T36), rabbit anti-AGO3 (abcam
281 ab154884), rabbit anti-AGO4 (CST, 6913), mouse anti-HaloTag (Promega, G921A), rabbit anti-DDX6
282 (Bethyl, A300-460A), rabbit anti-GW182 (Bethyl, A302-329A) (TNRC6A), mouse anti-Dicer (Abcam,
283 ab14601), mouse anti-alpha-Tubulin (GeneTex, GTX628802) and mouse anti-Histone H3 (Upstate, 05-
284 499). Anti-IgG horseradish peroxidase (Dako) and chemiluminescent detection (ThermoFisher
285 Scientific, Millipore WBKLS0500) were used to develop immunoblots. Blots were imaged on a GE
286 Healthcare ImageQuant imager. Densitometry of immunoblot band intensity was performed on
287 ImageJ, with target band intensity normalised to relative loading control intensity. Data represent
288 mean ± SEM of three independent experimental repeats.

289 ***Protein Co-Immunoprecipitation***

290 Cells from a 15 cm dish (one per elution) were lysed in 1 mL NP-40 buffer (150 mM NaCl, 50 mM Tris
291 pH 8.0, 0.7% NP-40, 5% Glycerol) supplemented with protease and phosphatase inhibitors before
292 centrifugation at 14,000 g for 5 minutes at 4 ºC to clear. After 80 µL of cleared lysate was taken for
293 input and mixed with 20 µL of 5X Laemmli buffer and boiled for 5 minutes, cleared lysate (1 mL) was
294 mixed with 1 µg of relevant antibody (Mouse IgA isotype control (eBioscience Invitrogen 14-4762-81)
295 and Mouse IgA anti-AGO2 (Santa-Cruz, sc-53521) and rotated at room temperature for 3 hours.
296 Protein L (Pierce, 88849) beads were washed twice in 500 µL of NP-40 buffer, resuspended in 30 µL of
297 NP-40 buffer, and then added to each IP. Samples were conjugated by rotating for 1.5 hours at room
298 temperature. Magnet bound samples were washed 4 times in 1 mL PBS with 0.1% Tween followed by
299 elution of protein complexes by addition of 40 µL of 0.2 M Glycine (pH 2.5) and 3 minutes incubation
300 at room temperature. Elutions were transferred to new tubes and neutralised with 5 µL of 1 M Tris-
301 HCl (pH 8). Following addition of 11.25 µL of 5X Laemmli buffer and boiling for 5 minutes, samples
302 were ready for analysis by western blot as described above.

303 ***Cell Fractionation***

304 Nuclear and cytoplasmic cell fractions were prepared as performed previously.[44] Following lysis of cells
305 with hypotonic lysis buffer, cells were incubated on ice for 10 minutes and centrifuged at 500 g for 5
306 minutes at 4 ºC. After supernatant was collected to form the cytoplasmic fraction, cell pellets were
307 washed for three minutes in 0.5 mL of hypotonic buffer three times. Nuclear membrane was lysed
308 with nuclear lysis buffer and sonicated for 20 seconds, followed by centrifugation at 15,000 g for 10
309 minutes at 4 ºC, with this supernatant forming the nuclear fraction. Samples were then prepared and
310 analysed by Western blot as described above.

311 ***Luciferase Reporter Assays***

nFor Firefly luciferase (FFLuc) silencing assays, cells were plated in 96 well plates. The following day cells were transfected using Attractene reagent (Qiagen, 301005) with 20ng/well pGL3 FFLuc, 10 ng/well pRLSV40 RLuc (expressing Renilla luciferase for normalisation), and 25 ng/well of esiRNA targeting either GFP (control) (Sigma, EHUEGFP) Scr control non-targeting pool siRNA (Horizon Discovery), or esiFFLuc (Sigma, EHUFLUC). After 48h, cells were harvested in 1X Passive Lysis Buffer and l and stored at -80°C. After thawing, FireFly and Renilla Luciferase activities were measured using the Dual-Luciferase Reporter Assay System (Promega, E1960) according to the manufacturer's instructions on a FLUOstar® Omega microplate reader.. Firefly luciferase activity was divided by the Renilla luciferase activity to normalise the data.

For assaying miR-100 silencing activity, we used the psiCheck2 miR-100 Targeting (T) and non-targeting (NT) reporters described in Bridge et al., 2017 (cite the cell reports 2017 paper here). Cells in 96 well plates were transfected with 20 ng of reporter plasmid, 20ng of AGO2 expression plasmid (or empty vector pEGFP-C1), and 15 nM of miR-100 microRNA mimic (Sigma) using Attractene transfection reagent (QIAGEN). 24 hours post-transfection, cells were harvested in 1X Passive Lysis buffer and luciferase activities assayed as above. Renilla luciferase activity was normalised by dividing by the Firefly luciferase activity.

MiR-451 RT-qPCR

TRIzol reagent (Invitrogen, 15596026) was used to isolate total RNA from cells at indicated confluency (log-phase = ∼60% confluency; confluent = ∼95% confluency) 60 hours after plating according to the manufacturer's instructions (with an additional 70% ethanol wash of RNA pellets). cDNA was generated from total RNA using the miRCURY LNA RT Kit (QIAGEN, 339340) and then amplified in duplicate by qPCR using the miRCURY LNA SYBR Green PCR Kit (QIAGEN, 339345) on a QuantStudio™ 5 Real-Time PCR machine (Applied Biosystems) with primers targeting *miR-451a* (QIAGEN, 3624799) and *U6* snRNA (v2) (QIAGEN, 3608295). *MiR-451a* CT values were normalized to *U6* and relative (to relevant WT) fold transcript abundance was calculated using the $2^{-\Delta\Delta Ct}$ method. Data represent mean ± SEM of two independent experimental repeats. To assay pri-miR-451, 1 µg of total RNA was treated with amplification grade DNase I (Sigma) according to the manufacturer's instructions. Diluted RNA was assayed using the Go-Taq 1-Step RT-qPCR system (Promega) for pri-miR-451 (Forward primer: GATGTACTAGTCCGGGCACC Reverse primer: TTGTGACAGGCTGAGCAGAG). *Beta Actin* mRNA was also assayed as a housekeeping gene using primers Forward: CTGGAACGGTGAAGGTGACG and Reverse: AAGGGACTTCCTGTAACAATGCA.

AGO2 WT RT-qPCR

To assay for untagged *AGO2* mRNA in our cells, total RNA was first extracted using TRIzol reagent according to the manufacturer's instructions. 1 µg of RNA was treated with amplification grade DNase I (Sigma) according to the manufacturer's instructions. A six-point serial dilution was prepared of RNA for generation of standard curves. Diluted RNA was assayed for *AGO2* transcript using the GoTaq 1-Step RT-qPCR System (Promega A6020) with primers CTGGCTCCAGGGGACAAG (Forward primer) and CCACTCGGTACACAATCGCT (Reverse primer). *Beta Actin* mRNA was also assayed as a housekeeping gene to normalise AGO2 transcript abundance. Primers were purchased from Integrated DNA Technologies.

Fluorescence Microscopy

353 Small round coverslips (1.5 thickness) in a 24 well plate were coated with sterile 0.1% gelatine and
354 then AGO2$^{-/-}$ A549 cells were plated. The following day 400 ng of plasmid (EGFP-VO, EGFP-AGO2 or
355 AGO2-EGFP) was transfected per well using DharmaFECT kb reagent (Horizon Discovery), according to
356 the manufacturer's instructions. 48h post-transfection, cells were fixed with 4% formaldehyde
357 solution in PBS for 10 minutes. Fixative was washed off with PBS three times and coverslips were
358 mounted onto a drop of mounting media containing DAPI (EverBrite™ Hardset Mounting Medium,
359 (biotium (#23004)) on glass slides, and cured in the dark overnight in preparation for imaging by
360 microscopy. For cells which underwent covalent protein labelling with HaloTag-TMR, prior to fixation
361 HaloTag® TMRDirect™ Ligand (Promega, G2991) was added to cell culture medium to a concentration
362 of 100 nM and incubated overnight. Cells were washed three times in fresh cell culture medium and
363 incubated for 30 minutes before a final wash, fixation and mounting. Slides were imaged with the
364 ZEISS LSM 880 with Airyscan confocal microscope (64 X oil objective).

365 ***Structural Analysis***

366 Atomic resolution structures of AGO2 were accessed via RCSB (https://www.rcsb.org). AlphaFold[45]
367 predictions of full-length AGO2 were taken from the DeepMind-EBI database
368 (https://alphafold.ebi.ac.uk; Access date: 08/2023). The structure of AGO2^{HALO} was predicted using
369 ColabFold v1.5.3.[46] Solvent accessible surfaces areas of AGO2 (PDB accession code, 4OLB) were
370 calculated using the POPScomp server (http://popscomp.org:3838/) using a solvent radius of 1.4 Å.[47]
371 Figures were made using PyMol (Schrodinger).

372 ***Statistical Analysis***

373 Statistical significance was calculated using the Student's t-test using GraphPad Prism 9.5.0 and is
374 represented as: not significant (ns) > 0.05; *p ≤ 0.05; **p ≤ 0.01; ***p ≤ 0.001 throughout. Data and
375 error bars represent mean ± SEM of three independent experimental repeats, unless otherwise stated.
376 Technical replicates (≥ 2) were performed in each independent experimental repeat for each sample
377 and condition where possible.

378

379

380 **Results**

381

382 **Creation and Genomic Characterisation of *AGO2^{HALO}* Cell Lines**

383 To investigate the functional activity of AGO2 fused at the C-terminus to HaloTag, we first generated
384 *AGO2^{HALO}* cells using CRISPaint technology. Following CRISPaint transfection of A549 cells, successful
385 editing should result in the insertion of HaloTag sequence (as well as sequence for a T2A site,
386 Puromycin resistance, and Poly(A) Tail) to the last exon of the endogenous *AGO2* locus (***Fig. 1A***). After
387 transfection, puromycin selection, and initial screening to confirm successful editing to fuse *AGO2*
388 with *HaloTag*, two untagged control (UnTagged *C1* (***UT C1***) and UnTagged *C2* (***UT C2***)) and two
389 *AGO2^{HALO}* (***AGO2^{HALO} C5*** *and* ***AGO2^{HALO} C10***)) clonal cell populations were selected for further
390 evaluation in this study alongside parental ***A549 WT*** cells. By selecting two *AGO2^{HALO}* and two
391 UnTagged CRISPaint control lines to compare against each other and to *WT* A549 cells we aspired to
392 accord greater confidence when interpreting results.

393 Amplification of genomic DNA (gDNA) revealed that, as expected, HaloTag sequence was only present
394 in *AGO2^{HALO}* clones (***Fig. 1B***). Sequencing of *AGO2^{HALO} C5* and *C10* cell populations identified two
395 *AGO2^{HALO}* variants, one long and one short (***Fig. 1C***). Mutations in the long variant replaced the final
396 two amino acids of AGO2 (FA) before the STOP codon of the *AGO2* sequence, while the shorter variant
397 had lost six amino acids (RTMYFA) before the Linker and *HaloTag* sequences. The two pairs of long
398 and short variant sequences are identical in both *AGO2^{HALO}* clones (***Fig. 1D***).[37,38,48]

399 Curiously, we observed amplification of *WT AGO2* sequence at the *AGO2-HaloTag* junction in both
400 *AGO2^{HALO}* clones (***Fig. 1B***), indicating retention of non-HaloTagged *AGO2* gDNA in edited *AGO2^{HALO}*
401 cells. Sequence alignments of these products identified an additional premature STOP codon (TAA) in
402 both *AGO2^{HALO}* clones (***Fig. 1E***). This slightly truncated *AGO2* sequence resulted in appreciable levels
403 of non-HaloTagged *AGO2* mRNA transcript in both *AGO2^{HALO}* clones (~40% of normalised *WT AGO2*
404 mRNA abundance in *A549 WT* cells) (***Fig. 1F***). Crucially, however, we did not observe any of this
405 truncated AGO2 during protein analysis of the lines by immunoblot (even at long exposures and

406 adjusted intensities) (***Fig. 1G***), suggesting the premature STOP codon results in very efficient
407 nonsense-mediated mRNA decay (NMD) of this transcript before translation.[49] Correspondingly,
408 immunoblot with anti-AGO2 and an anti-HaloTag antibody showed a band in the *AGO2^{HALO}* lines at 130
409 kDa, the correct predicted size for a fusion protein of AGO2 (97 kDa) and HaloTag (33 kDa), (***Fig. 1G-***
410 ***H***), confirming the HaloTag was fused with AGO2 in-frame and translated correctly. For the two
411 UnTagged clones 1 and 2, we performed sequencing of the genomic DNA at the end of the AGO2
412 coding sequence (***Supp Fig. 1B***) and found that no editing had occurred here, demonstrating that
413 *AGO2* coding sequence can be considered WT in these cells.

414 **Characterisation of Growth Rate and RISC Abundance in *AGO2^{HALO}* Cells**

415 As AGO2 is essential for many cell functions, we first probed whether C-terminal *AGO2^{HALO}* resulted in
416 changes to cell proliferation. The observed mean doubling time in *WT* cells of 26.5 ± 2.6 h was broadly
417 similar to that in both UnTagged (*UT C1* = 26.4 ± 0.8 h; *UT C2* = 30.6 ± 2.8 h) and *AGO2^{HALO}* cells
418 (*AGO2^{HALO} C5* = 28.4 ± 1.9 h; *AGO2^{HALO} C10* = 27.6 ± 1.8 h), with no statistically significant differences
419 observed and the greatest change (in relation to *WT*) detected in *UT C1* cells (***Fig. 2A***). These data
420 suggest *AGO2^{HALO}* fusion does not cause a discernible difference in cell proliferation rates (in this cell
421 line context), and that clonal selection has greater potential than *AGO2^{HALO}* fusion to influence cell
422 proliferation rate.

423 Due to potential compensatory effects arising from impaired AGO2 function in *AGO2^{HALO}* cells, we
424 considered whether the *AGO2^{HALO}* fusion resulted in changes in expression of other AGO proteins and
425 other proteins in the miRNA pathway (***Fig. 2B & C***). Densitometry of immunoblots (***Fig. 2D & E***) showed
426 that both *AGO2^{HALO}* clones continued to express other Argonaute family members (AGO1/3/4), the
427 core RISC proteins TNRC6A, DDX6, and proteins necessary for microRNA biogenesis and nuclear export
428 (Drosha, DGCR8, Dicer and Exportin 5). Although the abundance of TNRC6A, DDX6, remained stable
429 across lines, we did note increased AGO1 (not statistically significant), Dicer (not stastistically
430 significant) and AGO4 abundance (statistically significant rise from *WT* and *UT C1* to *AGO2^{HALO} C5* and

431 *C10*) in *AGO2^{HALO}* cells compared with WT and UnTagged cells. Speculatively, this could be due to
432 compensation/functional buffering occurring in *AGO2^{HALO}* cells to counter impaired AGO2 function.[50]
433 We also observed a decrease in AGO2 abundance in both *AGO2^{HALO}* lines compared with *WT* and *UT*
434 *C2*, but not *UT C1*, cells. As significant changes in protein abundance were also observed in UnTagged
435 clones compared to *WT*, we were unable to conclude if these decreases were caused directly by
436 *AGO2^{HALO}* fusion or clonal selection.

437 **AGO2^{HALO} Shows Reduced Binding to TNRC6A and Increased Binding to Dicer**

438 A core function of AGO2 is to bind other proteins involved in RNA processing and silencing to form a
439 complex to regulate translational control.[2,6] We explored whether AGO2^{HALO} can bind TNRC6A - a key
440 protein involved in miRNA-mediated silencing which acts to form a functional RISC when complexed
441 with AGO2[6] - and Dicer - a critical miRNA processing protein which cleaves precursor miRNAs to
442 generate mature miRNAs and which can also act as a platform for RISC assembly when complexed
443 with AGO2.[51] We performed immunoprecipitation of AGO2 from WT, UT C1, UT C2, AGO2^{HALO} C5 and
444 AGO2^{HALO}C10 cells (***Fig. 3A***). We observed greater levels of Dicer interacting with AGO2^{HALO} than with
445 untagged AGO2. On the other hand, TNRC6A strongly co-immunoprecipitated with AGO2 in WT and
446 UT clones but at reduced levels in the two AGO2-HaloTag clones. Of note, we did observe in elutions
447 for AGO2 immunoprecipitation, a faint band for WT AGO2 at 97 kDa in the AGO2^{HALO} lines, suggesting
448 that some WT AGO2 protein is produced from the AGO2 transcript that avoids nonsense-mediated
449 decay.

450 As mRNA translation is regulated temporally and spatially, correct sub-cellular localization of AGO2
451 and RISC is crucial for normal function. To investigate the sub-cellular localization of the AGO2 fusion
452 protein in *AGO2^{HALO}* cells compared with AGO2 in WT and UnTagged cells, we performed nuclear and
453 cytoplasmic fractionation (***Fig. 3B***). Our results show that there is much weaker (almost undetectable
454 at normal exposures) nuclear AGO2 signal in *AGO2^{HALO}* cells compared with WT and UnTagged clones.

455 Correspondingly, a clear signal for HaloTag was observed in cytoplasmic fractions of *AGO2*^{HALO} cells,
456 but not in the nuclear fraction of these cells.

457 The pre-eminent function of AGO2 in an active RISC is to correctly and efficiently pair miRNAs with
458 their targets to regulate mRNA translation. This can occur by direct cleavage of the mRNA by AGO2
459 after small RNA:mRNA binding (with perfect complementarity) or, where (partial or full) seed
460 matching is achieved, through a variety of alternative mechanisms which include recruitment of
461 TNRC6, CCR4-NOT, eIF4F inhibition, ribosome blocking, and mRNA decapping.[2]

462 To interrogate if *AGO2*^{HALO} fusion affected AGO2 cleavage function, we measured miR-451a
463 abundance in our cells. Unlike most miRNAs, maturation of the highly conserved vertebrate miR-451
464 bypasses Dicer, instead requiring direct cleavage of its precursor hairpin through catalytic AGO2 slicer
465 activity.[52,53,54,55] Due to this strict AGO2 slicer dependency, the presence of mature miR-451a in the
466 cell can demonstrate AGO2 catalytic function activity. We used RT-qPCR to quantify the normalized
467 abundance of miR-451a in WT, UnTagged, and AGO2^{HALO} cells (***Fig. 3C***). We found mature miR-451a
468 levels to be significantly decreased in the two AGO2^{HALO} clones when compared to WT and UnTagged
469 clones. By contrast, when we assayed the primary transcript for miR-451 (pri-miR-451), we observed
470 similar levels across all cell lines (***Fig. 3D***), indicating that the differences in mature miR-451a are not
471 due to differences in primary transcript abundance. The reduction in miR-451a abundance compared
472 with UnTagged control cells suggests C-terminal *AGO2*^{HALO} fusion resulted in significantly reduced miR-
473 451a biogenesis and therefore impaired AGO2 catalytic activity.

474 As measures of miR-451a abundance constitute only a qualified test for AGO2 cleavage function, we
475 performed further reporter gene-based functional assays. Using CRISPR-Cas9 editing, we generated
476 AGO2 knockout A549 cells (AGO2$^{-/-}$) to test alongside our WT, UnTagged and AGO2-HaloTag lines (***Fig.***
477 ***4A***). We more directly assayed AGO2 RNAi/slicer activity with a firefly luciferase (FFLuc) reporter gene
478 that can be targeted by esiRNA (***Fig. 4B***). esiRNA is a heterogenous mixture of siRNAs all of which are
479 fully complementary to the target sequence – FFLuc mRNA in this case. We found that in WT, UT C1

480 and UT C2 cells transfection of esiFFLuc resulted in a >50% reduction in normalized FFLuc activity
481 compared to where cells were transfected with esiRNA for GFP (a negative control), with no significant
482 difference between these lines. In the AGO2^{HALO}C5 and AGO2^{HALO}C10 lines, however, no such
483 repression of FFLuc activity was observed, with activity similar to that measured in AGO2$^{-/-}$ cells. This
484 result shows that AGO2 RNAi/slicer activity is completely impaired upon fusion of the HaloTag at the
485 C-terminal of AGO2.

486 To avoid any confounding effects of the deletions in AGO2 terminal amino acid residues we found
487 when sequencing the AGO2-HaloTag lines (***Fig. 1C-E***), and to facilitate direct comparison of AGO2 N
488 vs C-terminal tagging, we opted to create plasmid-based AGO2 fusions to EGFP that could be
489 transiently transfected into AGO2$^{-/-}$ cells. We cloned the full length AGO2 CDS into pEGFP-N1 or
490 pEGFP-C1 vectors to create C-terminally or N-terminally EGFP tagged AGO2, respectively. For AGO2-
491 EGFP, the linker between A859 of AGO2 and the M1 of EGFP is ADPPVAT, with no deletions of any
492 AGO2 residues. For EGFP-AGO2, the linker between K238 at the C-terminal of EGFP and M1 of AGO2
493 is SGLRSRAQAS, with no deletions of any AGO2 residues. We also made a construct expressing
494 untagged AGO2 by excising the EGFP cassette from pEGFP-C1 AGO2. As a control, we used the pEGFP-
495 C1 empty vector which only expresses EGFP (***Fig. 4C***). In AGO2$^{-/-}$ cells, we assessed FFLuc silencing by
496 esiFFLuc where EGFP-VO, AGO2 UT, EGFP-AGO2 or AGO2-EGFP had been co-transfected (***Fig. 4D***).
497 Transfection of AGO2 UT or EGFP-AGO2 yielded approximately 50% repression of FFLuc compared to
498 EGFP-VO transfected cells. AGO2-EGFP transfection, however, failed to cause significant FFLuc
499 repression, indicating an impairment AGO2 RNAi function.

500 Similar results were obtained when using miR-100 targeted (T) and non-targeted (NT) reporter
501 constructs to assay miR-100 mimic-mediated silencing (***Fig. 4E***): AGO2-EGFP did not cause additional
502 repression of the miR-100-targeted reporter when compared to EGFP-VO transfected cells, whereas
503 AGO2 UT and EGFP-AGO2 did. In EGFP-VO transfected AGO2$^{-/-}$ cells, the level of repression of the T
504 reporter was approximately 70% relative to the NT reporter, most likely due to miR-100 acting via
505 AGO1, 3 or 4 in these cells.

506 We next examined how untagged, N- and C-terminally tagged AGO2 partitioned in cytoplasmic and
507 nuclear fractions (***Fig. 4F***). All three were detected in cytoplasmic fractions, with the EGFP-tagged
508 proteins also detected by anti-GFP antibody. However, only untagged AGO2 and EGFP-AGO2 were
509 detected in the nuclear fractions, with AGO2-EGFP barely detectable. This partitioning mirrors that
510 observed for the C-terminal AGO2-HaloTag, which was also not detected in nuclear fractions (***Fig. 3B***).

511 To further investigate tagged AGO2 cellular localisation, we utilized the fluorescence signal of EGFP to
512 performe fluorescence microscopy in AGO2$^{-/-}$ A549 cells that had been transiently transfected with
513 EGFP-VO, EGFP-AGO2 or AGO2-EGFP (***Fig. 4G***). EGFP alone was distributed throughout the cell. For
514 EGFP-AGO2, we observed GFP signal in nuclear areas as well as in cytoplasmic foci that are reminiscent
515 of P-bodies. For AGO2-EGFP however, only a diffuse cytoplasmic signal was present, and no
516 cytoplasmic foci or nuclear localization were seen. Indeed, in imaging experiments on the AGO2-
517 HaloTag lines using the TMRDirect HaloTag ligand we found the signal from this ligand to be exclusively
518 cytoplasmic and diffuse (***Fig. 4H***).

519

520 **Discussion**

521

522 **CRISPaint Generated *AGO2^{HALO}* Cells have Comparable miRISC Core Protein Component**
523 **Abundancies and Cell Viability to WT.**

524 We successfully used CRISPaint technology to introduce a C-terminal *HaloTag* to *AGO2* to create
525 *AGO2^{HALO} A549* cells (***Fig. 1***). Two identical variants were identified in both *AGO2^{HALO}* clones, suggesting
526 selectivity for these two specific fusion events. We note that the specific sequence outcomes of fusion
527 events are hard to predict due to the potential for bases to be lost during repair. If precise fusion
528 occurs, the CRISPaint-*AGO2* targeting gRNA we employed would fuse AGO2 with a C-terminal HaloTag
529 with the loss of the three terminal amino acid residues of AGO2. WT human AGO2 is 859 residues
530 long. However, we identified two unique variants: "long", 857 residues; and "short", 853 residues.

531 Unexpectedly, we detected a non-HaloTagged AGO2 sequence (covering the gene-tag (*AGO2-*
532 *HaloTag*) junction) and appreciable levels of WT *AGO2* mRNA transcript in both *AGO2^{HALO}* clones. The
533 absence of observable non-HaloTagged AGO2 in *AGO2^{HALO}* cells by immunoblot, even at long
534 exposures and high input amounts, initially led us to conclude that these transcripts undergo efficient
535 NMD, presumably because of the two premature STOP codons.[49] However, we did not rule out that
536 some of this non-HaloTagged *AGO2* transcript may be translated into truncated AGO2 protein, even
537 if only stable for a short period. This was indeed observed later in our study, where we detected a
538 faint ~97 kDa AGO2 signal in our *AGO2^{HALO}* lines by immunoblot where AGO2 had been
539 immunoprecipitated (***Fig. 3A***). NMD has been shown to have a broad range of efficiency in cell
540 populations, with some cells degrading essentially all mRNAs while others escape NMD completely.[56]
541 It remains plausible that, due to the importance of functional AGO2 in the cell, there is survival
542 selection for *AGO2^{HALO}* CRISPaint clones which have less efficient NMD and therefore continue to
543 express (possibly at very low levels) WT (truncated) AGO2 protein. However, this argument is
544 somewhat clouded due to the known role of AGO2/RISC as an inhibitory regulator of NMD itself.[57,58]

545 Despite the retained expression of very low levels of non-HaloTagged AGO2 in *AGO2*^{HALO} lines, we
546 concluded from our immunoblots that the abundance of non-HaloTagged AGO2 protein in *AGO2*^{HALO}
547 was so low in comparison to the levels of AGO2 seen in WT and UnTagged cells that it would quickly
548 become saturated. Therefore, this truncated AGO2 would have minimal impact on silencing in the cell
549 and so our experiments evaluating silencing function in *AGO2*^{HALO} cells remain valid - especially given
550 that we observed disruption to, rather than retention of, function. The different variants and editing
551 events described herein likely reflect the specific hypotriploid karyotype of A549 cells and[59] the
552 challenge of creating multiple 'identical' edits of AGO2 in this complex and highly mutated genomic
553 context, re-emphasising the need for researchers to comprehensively define their tag-editing at the
554 DNA, RNA, and protein level.

555 Having validated the successful generation of *AGO2*^{HALO} fusion cells, we next sought to define the basic
556 characteristics of the cell. Due to the central nature of AGO2 in normal cell function, tagging of AGO2
557 may have resulted in differential proliferation. Indeed, down-regulation of *AGO2* has been associated
558 with cell proliferation and apoptosis in prostate cancer.[60] Encouragingly, our data indicated little
559 change in cell proliferation, with clonal selection potentially having a greater influence on proliferation
560 than *AGO2*^{HALO} fusion (***Fig. 2A***).

561 The first indication that C-terminal fusion of *AGO2*^{HALO} caused impairment to normal function was
562 noted from the observed increase in abundance of AGO1 and AGO4 in *AGO2*^{HALO} lines compared with
563 WT and UnTagged cells. This may be due to 'compensation' between Argonaute proteins following
564 defective AGO2 activity. It has been proposed that there is a degree of functional redundancy between
565 Argonaute proteins, where ablation or silencing of one Argonaute can be 'compensated' by other
566 Argonaute proteins.[3] For example, *AGO2* knock-out can result in increased AGO1 abundance, and vice
567 versa, and AGO3 levels were shown to increase in *AGO1*, *AGO2*, or *AGO1+AGO2* knock-out cells:
568 generally, *AGO* knock-out results in increased abundance of the remaining AGO proteins to maintain
569 overall AGO expression at a level near that of *WT*.[50] If *AGO2*^{HALO} fusion were to impair normal AGO2
570 function, the observed increase in AGO1/4 abundance (***Fig. 2B-C***) may be necessary to compensate

571 for the reduced silencing capacity of AGO2^{HALO}. We also considered that some changes may simply be
572 caused by clonal selection, highlighted by the significant reduction in AGO2 abundance in *UT C1* cells.

573 AGO2-HaloTag, in comparison to WT AGO2, exhibited reduced interaction with TNRC6A upon
574 immunoprecipitation (***Fig. 3A***). This critical binding partner is essential for miRNA mediated gene
575 silencing and normal miRISC function. Structural and interaction studies have shown that AGO2
576 interacts with tryptophan residues in TNRC6A via three tryptophan-binding pockets in the PIWI
577 domain (***Fig. 5D***).[61,62] Addition of the HaloTag may have disrupted the folding of the PIWI domain of
578 AGO2 rendering two of three of the Trp-binding pockets unable to interact with the tryptophan
579 residues on TRNC6A, thus impairing the interaction. The three tryptophan binding pockets on the
580 surface of the PIWI domain have been shown to act redundantly in binding tryptophan residues in
581 TNRC6B (PMID: 29576456). However, this study also showed that simultaneous mutation of two
582 pockets reduced interaction with the TRNC6B Ago-binding domain. In our AGO2 IP experiments, we
583 see a *reduced* interaction between AGO2-Halo and TNRC6A, not a total abolition, so it may be that
584 two of the tryptophan-binding pockets are misfolded with the addition of the C-terminal HaloTag.

585 Co-immunoprecipitation experiments also showed that, compared to WT AGO2, AGO2-HaloTag
586 exhibited greater interaction with Dicer, the protein that is essential for the maturation of almost all
587 miRNAs and the loading of small RNAs on to AGO2. Given the PIWI domain was also shown by others
588 to interact with Dicer,[63] we can speculate that the structure of the PIWI domain in AGO2-HaloTag still
589 retains the ability to interact with Dicer. Indeed, if TNRC6A and Dicer binding to AGO2 are mutually
590 exclusive, it may be that impairment of TRNC6A interaction leaves AGO2 more available to bind Dicer
591 in *AGO2^{HALO}* cells.

592

593 ***AGO2^{HALO}* Cells Have Significantly Impaired Cleavage and Silencing Function**

594 Ultimately, for C-terminal *AGO2^{HALO}* cells to act as a valuable platform to study AGO2 and RISC, data
595 must show that the key protein activities of slicing and miRNA-mediated silencing are sufficiently

596 retained. As such, we focussed on efficiently demonstrating and quantifying catalytic slicing by
597 measuring mature *miR-451a* abundance and RNAi of firefly luciferase in *AGO2*^{HALO} cells (***Fig. 3D; 4B***).

598 Although the presence of mature *miR-451a* (which strictly relies on AGO2 slicer dependency for
599 maturation) indicates some slicing function in *AGO2*^{HALO} cells, the significantly reduced (compared to
600 UnTagged cells) *miR-451a* abundance in *AGO2*^{HALO} cells suggests there is consequential deterioration
601 in AGO2 slicing ability arising from *AGO2*^{HALO} fusion.

602 To further explore impairment of AGO2 slicer function, we tested whether an esiRNA for firefly
603 luciferase could silence a firefly luciferase reporter gene transiently transfected into *AGO2*^{HALO} cells,
604 alongside *WT*, *UnTagged* and *AGO2*$^{-/-}$ cells (***Fig. 4B***). While in *WT* and *UnTagged* cells we observed
605 approximately 50% repression of firefly luciferase expression upon transfection of esiFFLuc, in
606 *AGO2*^{HALO} cells no repression of firefly luciferase expression was observed. This was also the case in
607 *AGO2*$^{-/-}$ cells, suggesting a near total impairment of AGO2 RNAi function in *AGO2*^{HALO} lines.

608 The *AGO2*^{HALO} cell lines we generated using CRISPaint editing and tag insertion led to deletion of some
609 amino acids at the C terminus of AGO2. The results we obtained showing functional impairment of
610 AGO2-HaloTag cannot therefore be specifically attributed to the C-terminal fusion of the tag or the
611 loss of the C -terminal amino acids. Creation and use of the EGFP-tagged plasmid constructs, which
612 resulted in no deletion of residues from AGO2, therefore reduced any ambiguity that C-terminal
613 tagging itself impairs AGO2 function and localisation, as well as providing greater clarity that C-
614 terminal tagging is more deleterious than N-terminal tagging of AGO2. Utilising our *AGO2*$^{-/-}$ *A549* as a
615 'clean' background, we directly compared the function of N- and C-terminally tagged AGO2
616 exogenously expressed from transfected plasmid constructs. We used the EGFP tag as it is of similar
617 size to HaloTag and permits straightforward visualization. The firefly luciferase RNAi assay confirmed
618 that a C-terminally tagged AGO2 is impaired in RNAi function (***Fig. 4D***) and we also found that miRNA
619 (miR-100)-mediated silencing is similarly abrogated (***Fig. 4E***). Notably, N-terminally EGFP tagged AGO2
620 performed as well as an untagged form of AGO2 in these assays, indicating that core AGO2 function

621 is maintained, and demonstrating there is less disruption to AGO2 function when tags are added to
622 the N- rather than C-terminus..

623 Comparison of our reporter data with previously published evidence of the effect of N-terminal
624 *HaloTag-Ago2* fusion in MEFs – noting the different model systems and editing tools used - indicates
625 that C-terminal *AGO2*^{HALO} or EGFP fusion in A549 cells results in greater impairment to silencing
626 function. Dual-Luciferase reporter experiments which were related, but not interchangeable, to ours
627 did not show measurable differences in repression between WT and *Ago2*$^{Halo/Halo}$ MEFs for three
628 miRNA binding site containing constructs (*PTEN* 3' UTR *miR-29* binding site; *Adrb2* 3' UTR *let-7* binding
629 site; *Taf7* 3' UTR *miR-21* binding site), though these experiments did not knock-down or perturb active
630 Ago2 and so specific differences between Ago2 and HaloTag-Ago2 activity may not have been
631 assessed.[14] These findings were re-affirmed by a sensitive two-colour fluorescent reporter system.[14]
632 Notably, however, the N-terminal *HaloTag-Ago2* fusion did result in notable functional defects
633 including relative derepression of miRNA targets, reduced viability of homozygous mice, and reduced
634 ability to rescue RNAi in *Ago2*$^{-/-}$ MEFs compared with WT Ago2.[14]

635 Notwithstanding, in both comparative and absolute terms our data led us to conclude that C-
636 terminally fused *AGO2*^{HALO} cells have significantly impaired endogenous AGO2-mediated silencing
637 function compared to *WT* and *UnTagged* cells. This evidence of such impairment to AGO2 silencing
638 caused by C-terminal fusion of *AGO2*^{HALO} does not support C-terminal *AGO2*^{HALO} as a suitable model
639 for the study of AGO2 and RISC biology. Regarding the validation of tagged AGO2, we urge for
640 increased use of orthogonal standardised and reproducible (where possible) experimental measures
641 of AGO2 silencing capacity. We believe this will ensure comparability between studies (and
642 tags/tagging strategies), as well as ultimately saving researchers valuable time and resources.

643

644 **A Molecular Explanation for Impairment of AGO2 by Addition of a C-terminal HaloTag**

645 Inspection of the 3D structure of human AGO2[51,64] provides insight as to why a C-terminal HaloTag
646 impairs activity. Protein termini are typically solvent exposed,[65] however, the C-terminus of AGO2 is
647 an uncommon example where the last residue is buried (only 20% of the surface area of A859 is
648 accessible to a solvent probe with radius 1.4 Å). The buried carboxylate group of A859 also forms
649 functionally relevant interactions (***Fig. 5A***), including hydrogen bonds with several residues (e.g. K556
650 and R792) that themselves interact with the phosphate groups of residues 1 and 3 of the miRNA.
651 Moreover, in some of the reported structures, the carboxylate groups of Y857 and A859 interact with
652 a buried water molecule that also interacts with the 5' terminal phosphate group of the miRNA.
653 Evidently, modification of the sequence in this region of the protein via deletion of native residues and
654 addition of a HaloTag will likely perturb the RNA binding properties of AGO2 (***Fig. 5B***). Indeed,
655 prediction of the AGO2^{HALO} structure using AlphaFold2 shows the linker region between AGO2 and the
656 HaloTag exiting AGO2 via the miRNA binding site (data not shown). While the confidence (both pLDDT
657 and PAE) for this region of the model is low, this prediction is consistent with our experimental data.

658 By contrast, the N-terminus of AGO2 is solvent exposed (***Fig. 5D***), which is consistent with previously
659 reported successful tagging of this end of the protein for both *in vitro* and in cell studies. Indeed,
660 crystal structures of AGO2 tend to lack data for the first 20-25 residues,[51,64] presumably due to the
661 inherent flexibility of this region. Prediction of the structure of full-length AGO2 using AlphaFold2[45]
662 shows low confidence for the first 25 residues, consistent with this region being flexible and solvent-
663 exposed.[66]

664 **Distinct Sub-Cellular Localisation of AGO2^{HALO}**

665 For proteins to function normally, they must localise correctly. We determined from our imaging and
666 fractionation data that sub-cellular localisation of AGO2 is significantly altered as a result of the C-
667 terminal fusion, with a much-reduced nuclear localisation of the AGO2 fusion protein in *AGO2^{HALO}* cells
668 (***Figs 3A and 4H***). Nuclear and cytoplasmic fractionation and imaging experiments also revealed that

669 AGO2-EGFP was similarly absent in the nucleus compared to untagged AGO2 and EGFP-AGO2 (***Fig. 4F***
670 ***and G***), suggesting this is an effect specific to C-terminal AGO2 tagging.

671 Notably, *Ago2*$^{-/-}$ MEFs expressing an N-terminal HaloTag-Ago2 fusion were also found to show a
672 prevalently cytoplasmic localisation of the fusion protein,[14] though it is unclear if this differs from the
673 signal present in WT cells due to a lack of direct comparison. Impaired nuclear localisation could arise
674 for many reasons, most obviously perhaps due to the addition of the large (33 kDa) HaloTag preventing
675 binding of mediators of nuclear import.[67,68] It may also be the case that loss of the carboxylate group
676 of A859 specifically disrupts the structure of AGO2 in a way that impairs binding to nuclear import
677 factors. Factors that regulate nuclear import of AGO2 continue to be revealed[69,70] and it may be that
678 the PIWI domain and/or the C-terminal region are more critical in these interactions than is currently
679 understood. Further studies with deletion mutants of AGO2 would help define the critical residues
680 and structural motifs. Although RISC activity has been considered primarily cytoplasmic, and our
681 principal research intention was to use *AGO2*^{HALO} to investigate (primarily) cytoplasmic RISC activity,
682 nuclear RISC has been shown to regulate both transcriptional rates and post-transcriptional mRNA,
683 and RNAi factors are known to be present and functional in human cell nuclei.[71,72,72,73,74] Moreover, a
684 shift in localization of AGO2 from cytoplasm to nucleus was recently shown to derepress cytoplasmic
685 AGO2-eCLIP targets that were candidates for canonical regulation by miRISC.[75] Therefore, the
686 potential downstream effects of disrupted nuclear localisation should not be overlooked when
687 considering *AGO2*^{HALO} as a model for studying AGO2/RISC.

688 Previous studies have shown that there is a greater, but comparable, concentration of nuclear and
689 cytoplasmic AGO2 in A549 cells and generally a nuclear to cytoplasmic ratio below one in most cell
690 types.[74,76] Our fractionation data is congruent with this, with comparable levels of AGO2 observed in
691 both fractions of *A549 WT* cells. Interestingly, tagged AGO2 has previously been shown to result in
692 altered AGO2 protein localisation. N-terminal tagged FLAG-AGO2 exhibited shifted nuclear and
693 cytoplasmic distribution (approximately equal for endogenous AGO2 in T47D cells compared with 67%
694 cytoplasmic and 33% nuclear in *FLAG-AGO2* over-expressing cells),[8] although this change could be

695 more a consequence of high (5-fold) ectopic overexpression, rather than directly attributable to the
696 tag itself. Similarly, immunofluorescence images of *MYC-AGO2* U2-OS cells stained with FITC-
697 conjugated anti-Myc showed a predominantly cytoplasmic Myc-AGO2 signal with prevalent
698 cytoplasmic foci, while endogenous AGO2 showed a predominantly nuclear signal – it remains unclear
699 if these differences arise directly from the Myc-tag or non-specific antibody binding.[77,78]

700 Together with our reporter assays indicating significantly impaired silencing function, the distinct sub-
701 cellular localisation of C-terminally tagged AGO2 convinced us to reject both C-terminal *AGO2*^{HALO}
702 fusion and C-terminal AGO2-EGFP as a viable tool for study of AGO2/RISC.

703

704 **Conclusion**

705 The capacity to investigate the mechanisms behind biological processes and disease has been greatly
706 enhanced by the ability to produce proteins of interest fused to relevant tags. However, every tag
707 added to a protein has the potential to impede functionality, which may invalidate any experimental
708 conclusions. As a result, careful tag design together with reliable and reproducible validation
709 experiments are essential for advancing (miRNA-silencing) research. This is especially important for
710 proteins like AGO2, which often function as part of larger complexes and have numerous and diverse
711 roles and activities. Concerningly, several previous studies that have used tagged forms of AGO2 to
712 investigate AGO2/RISC have not adequately demonstrated, either through published tag validation or
713 the lack thereof, that core functions of tagged AGO2 are sufficiently maintained. As even small
714 modifications can have functional consequences, this shortfall in validation casts doubt on the validity
715 of some of these findings. Additionally, the paucity of AGO2 antibody validation presents a risk of
716 artificial results arising from non-specific binding of antibodies used to probe AGO2. Therefore, to
717 ensure the validity and robustness of future AGO2/RISC investigational findings, we recommend more
718 comprehensive protein-tag (and antibody) validation work to be performed and published in detail
719 alongside investigational findings.

720

721 We constructed C-terminal *AGO2*^{HALO} fusion cells to investigate if AGO2^{HALO} was a suitable model for
722 studying RISC biology in human cells. Our research revealed that, while AGO2^{HALO} retained some
723 capacity to form native protein-protein interactions, *AGO2*^{HALO} cells displayed distinct sub-cellular
724 localization and significantly reduced silencing function compared to normal AGO2. This loss of
725 function led us to conclude that C-terminal fusion of *AGO2*^{HALO} was not appropriate for further
726 research into the biology of AGO2/RISC. Moreover, we showed that similar loss of silencing function
727 and aberrant localisation occurs in cells transfected with a C-terminal AGO2-EGFP plasmid, but not N-
728 terminal EGFP-AGO2, suggesting C-terminal tagging of AGO2 in general is inappropriate and N-
729 terminal tagging is more desirable.

730

731 While this study establishes important insights into the consequences of C-terminal HaloTag fusion on
732 AGO2 functionality, several limitations should be noted. First, the endogenous tagging data focussed
733 exclusively on the HaloTag — a relatively large (33 kDa) tag — in a single C-terminal configuration,
734 while the N- vs C-terminal AGO2 exogenous tag comparison data is directly relevant for EGFP only (27
735 kDa) . Given AGO2's complex domain structure and critical roles within RISC, alternative tags or
736 placements may yield different functional outcomes. Exploring smaller tags or N-terminal fusions
737 could potentially mitigate some of the disruptions observed here and is a recommended avenue for
738 future study.

739

740 Ultimately, we hope that our work serves as a valuable case study to underscore the importance of
741 careful validation of all core protein competencies of recombinantly tagged proteins. We strongly
742 encourage future research using N-terminal (or any) AGO2 tag fusions to conduct and publish
743 comprehensive validation assays. It is crucial to avoid relying on any single assay and, instead, perform
744 a combination of experiments (e.g., Luciferase reporter assays, *miR-451a*/slicing assays, co-

745 immunoprecipitation/protein-interaction experiments, and localization studies) to validate the range
746 of core protein functionalities, thereby increasing confidence in investigational findings.. A
747 community-wide effort to ensure only the most robustly validated reagents and methods are used to
748 characterise AGO2 and RISC biology would enable the miRNA community to gain valuable insights into
749 RNA silencing biology of greater scientific rigour. More broadly, the availability of AlphaFold models
750 for 220 million proteins means that the design of fusion proteins can now be guided by atomic
751 resolution predictions of protein structure in the absence of experimental data. We therefore strongly
752 recommend well-thought-out design and validation strategies to enhance our understanding of the
753 impact of specific tags and tagging strategies on protein function.

754

755 Funding
756 This work was supported by funds awarded to T.V.S. from the BBSRC (Grant Code BB/V009567/1).

757 Author contributions
758 K.M.S., A.F.F.C, A.A, M.J.P ,P.G. and T.V.S. designed and performed experiments and analysed the data.
759 A.A and M.A. provide invaluably technical and experimental assistance. All authors contributed to
760 editing and proofreading the manuscript. K.M.S., A.F.F.C, M.J.P., and T.V.S. wrote the manuscript.
761 T.V.S. supervised and managed all research.

762 Acknowledgements
763 We would like to acknowledge the advice and helpful discussions and additional editorial
764 suggestions of this work/investigation from Prof. Dimitris Lagos, Dr Faraz Mardakheh and Dr Paulo S.
765 Ribeiro.

766

767 **References**
768

769 1. Hutvagner, G. & Simard, M. J. Argonaute proteins: Key players in RNA silencing. *Nature*
770 *Reviews Molecular Cell Biology* **9**, 22–32 (2008).

771 2. Frédérick, P. M. & Simard, M. J. Regulation and different functions of the animal microRNA-
772 induced silencing complex. *Wiley Interdisciplinary Reviews: RNA* 1–22 (2021)
773 doi:10.1002/wrna.1701.

774 3. Huntzinger, E. & Izaurralde, E. Gene silencing by microRNAs: Contributions of translational
775 repression and mRNA decay. *Nature Reviews Genetics* **12**, 99–110 (2011).

776 4. Behm-Ansmant, I. *et al.* mRNA degradation by miRNAs and GW182 requires both CCR4:NOT
777 deadenylase and DCP1:DCP2 decapping complexes. *Genes and Development* **20**, 1885–1898
778 (2006).

779 5. Chekulaeva, M. *et al.* MiRNA repression involves GW182-mediated recruitment of CCR4-NOT
780 through conserved W-containing motifs. *Nature Structural and Molecular Biology* **18**, 1218–
781 1226 (2011).

782 6. Lian, S. L. *et al.* The C- Terminal half of human Ago2 binds to multiple GW- rich regions of
783 GW182 and requires GW182 to mediate silencing. *Rna* **15**, 804–813 (2009).

784 7. Liu, J. *et al.* A role for the P-body component GW182 in microRNA function. *Nature Cell*
785 *Biology* **7**, 1161–1166 (2005).

786 8. Roya, K. *et al.* Stable association of RNAi machinery is conserved between the cytoplasm and
787 nucleus of human cells. *Rna* **22**, 1085–1098 (2016).

788 9. Mauro, M., Berretta, M., Palermo, G., Cavalieri, V. & Rocca, G. La. Special Section on Non-
789 Coding RNAs in Clinical Practice : From Biomarkers to Therapeutic Tools — Minireview The
790 Multiplicity of Argonaute Complexes in Mammalian Cells. *THE JOURNAL OF PHARMACOLOGY*
791 *AND EXPERIMENTAL THERAPEUTICS* 52–60 (2023) doi:10.1124.

792 10. Kedersha, N. & Anderson, P. Mammalian Stress Granules and Processing Bodies. *Methods in*
793 *Enzymology* **431**, 61–81 (2007).

794 11. Gibson, T. J., Seiler, M. & Veitia, R. A. The transience of transient overexpression. *Nature*
795 *Methods* **10**, 715–721 (2013).

796 12. Booth, W. T. *et al.* Impact of an N-terminal polyhistidine tag on protein thermal stability. *ACS*
797 *Omega* **3**, 760–768 (2018).

798 13. La Rocca, G. *et al.* In vivo, Argonaute-bound microRNAs exist predominantly in a reservoir of
799 low molecular weight complexes not associated with mRNA. *Proceedings of the National*
800 *Academy of Sciences of the United States of America* **112**, 767–772 (2015).

801 14. Li, X. *et al.* High-Resolution In Vivo Identification of miRNA Targets by Halo-Enhanced Ago2
802 Pull-Down. *Molecular Cell* **79**, 167-179.e11 (2020).

803 15. Horman, S. R. *et al.* Akt-mediated phosphorylation of argonaute 2 downregulates cleavage
804 and upregulates translational repression of MicroRNA targets. *Molecular Cell* **50**, 356–367
805 (2013).

806 16. Gurard-levin, Z. A., Kilian, K. A., Kim, J. & Ba, K. HaloTag: A Novel Protein Labeling Technology
807 for Cell Imaging and Protein Analysis. *ACS Chemical Biology* **60**, 45–58 (2010).

808 17. England, C. G., Luo, H. & Cai, W. HaloTag Technology: A Versatile Platform for Biomedical
809 Applications. *Bioconjugate Chemistry* **26**, 975–986 (2015).

810 18. Chen, W., YOUNIS, M. H., Zhao, Z. & Cai, W. Recent biomedical advances enabled by HaloTag
811 technology. *Biocell* **46**, 1789–1801 (2022).

812 19. Gu, J. *et al.* GoldCLIP: Gel-omitted Ligation-dependent CLIP. *Genomics, Proteomics and*
813 *Bioinformatics* **16**, 136–143 (2018).

814 20. Guo, J. K. *et al.* Denaturing purifications demonstrate that PRC2 and other widely reported
815 chromatin proteins do not appear to bind directly to RNA in vivo. *Mol Cell* **84**, 1271-1289.e12
816 (2024).

817 21. Hafner, M. *et al.* CLIP and complementary methods. *Nature Reviews Methods Primers* **1**,
818 (2021).

819 22. Grimm, J. B. *et al.* A general method to improve fluorophores for live-cell and single-molecule
820 microscopy. *Nature Methods* **12**, 244–250 (2015).

821 23. Duc, H. & Ren, X. Labelling HaloTag Fusion Proteins with HaloTag Ligand in Living Cells. *Bio-*
822 *Protocol* **7**, 1–8 (2017).

823 24. Kompa, J. *et al.* Exchangeable HaloTag Ligands (xHTLs) for multi-modal super-resolution
824 fluorescence microscopy. *J. Am. Chem. Soc.* 2022.06.20.496706 (2022)
825 doi:10.1021/jacs.2c11969.

826 25. Kwak, P. B. & Tomari, Y. The N domain of Argonaute drives duplex unwinding during RISC
827 assembly. *Nature Structural and Molecular Biology* **19**, 145–151 (2012).

828 26. Ma, J. B., Ye, K. & Patel, D. J. Structural basis for overhang-specific small interfering RNA
829 recognition by the PAZ domain. *Nature* **429**, 318–322 (2004).

830 27. Gu, S., Jin, L., Huang, Y., Zhang, F. & Kay, M. A. Slicing-independent RISC activation requires
831 the argonaute PAZ domain. *Current Biology* **22**, 1536–1542 (2012).

832 28. Boland, A., Huntzinger, E., Schmidt, S., Izaurralde, E. & Weichenrieder, O. Crystal structure of
833 the MID-PIWI lobe of a eukaryotic argonaute protein. *Proceedings of the National Academy*
834 *of Sciences of the United States of America* **108**, 10466–10471 (2011).

835 29. Parker, J. S., Roe, S. M. & Barford, D. Structural insights into mRNA recognition from a PIWI
836 domain-siRNA guide complex. *Nature* **434**, 663–666 (2005).

837 30. Song, J. J., Smith, S. K., Hannon, G. J. & Joshua-Tor, L. Crystal structure of argonaute and its
838 implications for RISC slicer activity. *Science* **305**, 1434–1437 (2004).

839 31. Parker, J. S., Roe, S. M. & Barford, D. Crystal structure of a PIWI protein suggests mechanisms
840 for siRNA recognition and slicer activity. *EMBO Journal* **23**, 4727–4737 (2004).

841 32. Ma, J. B. *et al.* Structural basis for 5′ -end-specific recognition of guide RNA by the A. fulgidus
842 Piwi protein. *Nature* **434**, 666–670 (2005).

843 33. Rivas, F. V. *et al.* Purified Argonaute2 and an siRNA form recombinant human RISC. *Nature*
844 *Structural and Molecular Biology* **12**, 340–349 (2005).

845 34. Kang, H. W., Tabata, Y. & Ikada, Y. Fabrication of porous gelatin scaffolds for tissue
846 engineering. *Biomaterials* (1999) doi:10.1016/S0142-9612(99)00036-8.

847 35. Yuan, Y. R. *et al.* Crystal structure of A. aeolicus argonaute, a site-specific DNA-guided
848 endoribonuclease, provides insights into RISC-mediated mRNA cleavage. *Molecular Cell* **19**,
849 405–419 (2005).

850 36. Nakanishi, K., Weinberg, D. E., Bartel, D. P. & Patel, D. J. Structure of yeast Argonaute with
851 guide RNA. *Nature* **486**, 368–374 (2012).

852 37. Nakanishi, K. Critical Reviews and Perspectives Anatomy of four human Argonaute proteins.
853 1–21 (2022).

854 38. Müller, M., Fazi, F. & Ciaudo, C. Argonaute Proteins: From Structure to Function in
855 Development and Pathological Cell Fate Determination. *Frontiers in Cell and Developmental*
856 *Biology* **7**, 1–10 (2020).

857 39. Hauptmann, J. *et al.* Turning catalytically inactive human Argonaute proteins into active slicer
858 enzymes. *Nature Structural and Molecular Biology* **20**, 814–817 (2013).

859 40. Schürmann, N., Trabuco, L. G., Bender, C., Russell, R. B. & Grimm, D. Molecular dissection of
860 human Argonaute proteins by DNA shuffling. *Nature Structural and Molecular Biology* **20**,
861 818–826 (2013).

862 41. Hur, J. K., Zinchenko, M. K., Djuranovic, S. & Green, R. Regulation of Argonaute slicer activity
863 by guide RNA 3' end interactions with the N-terminal lobe. *Journal of Biological Chemistry*
864 **288**, 7829–7840 (2013).

865 42. Mukherji, S. *et al.* MicroRNAs can generate thresholds in target gene expression. *Nature*
866 *Genetics* **43**, 854–859 (2011).

867 43. Schmid-Burgk, J. L., Höning, K., Ebert, T. S. & Hornung, V. CRISPaint allows modular base-
868 specific gene tagging using a ligase-4-dependent mechanism. *Nature Communications* **7**,
869 (2016).

870 44. Liu, Z., Johnson, S. T., Zhang, Z. & Corey, D. R. Expression of TNRC6 (GW182) Proteins Is Not
871 Necessary for Gene Silencing by Fully Complementary RNA Duplexes. *Nucleic Acid*
872 *Therapeutics* **29**, 323–334 (2019).

873 45. Jumper, J. *et al.* Highly accurate protein structure prediction with AlphaFold. *Nature* **596**,
874 583–589 (2021).

875 46. Mirdita, M. *et al.* ColabFold: making protein folding accessible to all. *Nature Methods* **19**,
876 679–682 (2022).

877 47. Cavallo, L., Kleinjung, J. & Fraternali, F. POPS: A fast algorithm for solvent accessible surface
878 areas at atomic and residue level. *Nucleic Acids Research* **31**, 3364–3366 (2003).

879 48. Elkayam, E. *et al.* The structure of human argonaute-2 in complex with miR-20a. *Cell* **150**,
880 100–110 (2012).

881 49. Hug, N., Longman, D. & Cáceres, J. F. Mechanism and regulation of the nonsense-mediated
882 decay pathway. *Nucleic Acids Research* **44**, 1483–1495 (2015).

883 50. Johnson, K. C., Johnson, S. T., Liu, J. & Chu, Y. Prioritizing Annotated miRNAs : Only a Small
884 Percentage are Candidates for Biological Regulation. (2022).

885 51. Chendrimada, T. P. *et al.* TRBP recruits the Dicer complex to Ago2 for microRNA processing
886 and gene silencing. *Nature* **436**, 740–744 (2005).

887 52. Cheloufi, S., Dos Santos, C. O., Chong, M. M. W. & Hannon, G. J. A dicer-independent miRNA
888 biogenesis pathway that requires Ago catalysis. *Nature* **465**, 584–589 (2010).

889 53. Cifuentes, D. *et al.* A novel miRNA processing pathway independent of dicer requires
890 argonaute2 catalytic activity. *Science* **328**, 1694–1698 (2010).

891 54. Yang, S. *et al.* Conserved vertebrate mir-451 provides a platform for Dicer-independent,
892 Ago2-mediated microRNA biogenesis. *Proceedings of the National Academy of Sciences of the*
893 *United States of America* **107**, 15163–15168 (2010).

894 55. Kretov, D. A. *et al.* Ago2-Dependent Processing Allows miR-451 to Evade the Global
895 MicroRNA Turnover Elicited during Erythropoiesis. *Molecular Cell* **78**, 317-328.e6 (2020).

896 56. Sato, H. & Singer, R. H. Cellular variability of nonsense-mediated mRNA decay. *Nature*
897 *Communications* **12**, 1–12 (2021).

898 57. Choe, J., Cho, H., Lee, H. C. & Kim, Y. K. MicroRNA/Argonaute 2 regulates nonsense-mediated
899 messenger RNA decay. *EMBO Reports* **11**, 380–386 (2010).

900 58. Choe, J., Cho, H., Chi, S. G. & Kim, Y. K. Ago2/miRISC-mediated inhibition of CBP80/20-
901 dependent translation and thereby abrogation of nonsense-mediated mRNA decay require
902 the cap-associating activity of Ago2. *FEBS Letters* **585**, 2682–2687 (2011).

903 59. Park, S. Y., Choi, H. C., Chun, Y. H., Kim, H. & Park, S. H. Characterization of chromosomal
904 aberrations in lung cancer cell lines by cross-species color banding. *Cancer Genetics and*
905 *Cytogenetics* **124**, 62–70 (2001).

906 60. Bian, X. J. *et al.* Down-regulation of Dicer and Ago2 is associated with cell proliferation and
907 apoptosis in prostate cancer. *Tumor Biology* **35**, 11571–11578 (2014).

908 61. Schirle, N. T. & MacRae, I. J. The crystal structure of human argonaute2. *Science (1979)* **336**,
909 1037–1040 (2012).

910 62. Sheu-Gruttadauria, J. & MacRae, I. J. Phase Transitions in the Assembly and Function of
911 Human miRISC. *Cell* **173**, 946-957.e16 (2018).

912 63. Tahabaz, N. *et al.* Characterization of the interactions between mammalian PAZ PIWI domain
913 proteins and Dicer. *EMBO Rep* **5**, 189–194 (2004).

914 64. Schirle, N. T. & MacRae, I. J. The crystal structure of human argonaute2. *Science* **336**, 1037–
915 1040 (2012).

916 65. Jacob, E. & Unger, R. A tale of two tails: Why are terminal residues of proteins exposed?
917 *Bioinformatics* **23**, 225–230 (2007).

918 66. Akdel, M. *et al.* A structural biology community assessment of AlphaFold2 applications.
919 *Nature Structural and Molecular Biology* **29**, 1056–1067 (2022).

920 67. Sallis, S., Grondin, B., Leduc, E., Azouz, F. & Pilon, N. FAM172A controls the nuclear import
921 and alternative splicing function of AGO2. *bioRxiv* (2022).

922 68. Schraivogel, D. *et al.* Importin-β facilitates nuclear import of human GW proteins and
923 balances cytoplasmic gene silencing protein levels. *Nucleic Acids Research* **43**, 7447–7461
924 (2015).

925 69. Weinmann, L. *et al.* Importin 8 Is a Gene Silencing Factor that Targets Argonaute Proteins to
926 Distinct mRNAs. *Cell* **136**, 496–507 (2009).

927 70. Sallis, S. *et al.* The CHARGE syndrome-associated protein FAM172A controls AGO2 nuclear
928 import. *Life science alliance* **6**, 1–15 (2023).

929 71. O'Brien, J., Hayder, H., Zayed, Y. & Peng, C. Overview of microRNA biogenesis, mechanisms of
930 actions, and circulation. *Frontiers in Endocrinology* **9**, 1–12 (2018).

931 72. Nishi, K., Nishi, A., Nagasawa, T. & Ui-Tei, K. Human TNRC6A is an Argonaute-navigator
932 protein for microRNA-mediated gene silencing in the nucleus. *Rna* **19**, 17–35 (2013).

933 73. Pitchiaya, S., Heinicke, L. A., Park, J. I., Cameron, E. L. & Walter, N. G. Resolving Subcellular
934 miRNA Trafficking and Turnover at Single-Molecule Resolution. *Cell Reports* **19**, 630–642
935 (2017).

936 74. Gagnon, K. T., Li, L., Chu, Y., Janowski, B. A. & Corey, D. R. RNAi factors are present and active
937 in human cell nuclei. *Cell Reports* **6**, 211–221 (2014).

938 75. Johnson, K. C., Kilikevicius, A., Hofman, C., Hu, J. & Liu, Y. Nuclear Localization of Argonaute is
939 affected by Cell Density and May Relieve Repression by microRNAs. (2023).

940 76. Sarshad, A. A. *et al.* Argonaute-miRNA Complexes Silence Target mRNAs in the Nucleus of
941 Mammalian Stem Cells. *Molecular Cell* **71**, 1040-1050.e8 (2018).

942 77. Liu, J., Valencia-Sanchez, M. A., Hannon, G. J. & Parker, R. MicroRNA-dependent localization
943 of targeted mRNAs to mammalian P-bodies. *Nature Cell Biology* **7**, 719–723 (2005).

944 78. Van Eijl, R. A. P. M., Van Den Brand, T., Nguyen, L. N. & Mulder, K. W. Reactivity of human
945 AGO2 monoclonal antibody 11A9 with the SWI/SNF complex: A case study for rigorously
946 defining antibody selectivity. *Scientific Reports* **7**, 1–11 (2017).

947

948

Figure Legends

Figure 1. Creation and Genomic Characterisation of AGO2-HaloTag Cell Lines
(A) Schematic of WT AGO2 and the C terminal AGO2-HaloTag fusion (including T2A site, Puromycin resistant (PuroR) and Poly(A) sections) genotype to be generated by CRISPaint editing of A549 cells. Arrows indicate locations of forward and reverse primers designed to confirm editing. Blue = *AGO2* WT last intron Forward and Reverse; Light Teal = HaloTag1 Forward and Reverse; Dark Teal = HaloTag2 Forward and Reverse. (B) Agarose gel loaded with PCR products of A549 WT and two *AGO2-HaloTag* (*AGO2-HaloTag C5* and *AGO2-HaloTag C10*) lines amplified with indicated combinations of *AGO2* WT and *HaloTag* primers, as indicated in (A). Red arrows indicate gDNA containing *HaloTag* sequence which was purified and submitted for sequencing. Circled numbers 1-3 indicate gDNA containing C terminal non-HaloTagged *AGO2* product which was purified and submitted for sequencing. (C) Sequence (generated from TOPO-seq) alignments of *WT* and two *AGO2-HaloTag* clones at the AGO2-HaloTag junction. From several submitted TOPO clones, two variants of *AGO2-HaloTag* (one long and one short) were identified in *AGO2-HaloTag* cells. Asterisk (*) indicates STOP codon. (D) Schematic to show known functionally important domains of AGO2, with a focus on C-terminal PIWI domain. CRISPaint mediated AGO2-HaloTag fusion generated a long and a short variant, neither of which resulted in loss of residues known to have functional importance. (E) Chromatograph of C terminal *AGO2* sequence identified in WT, *AGO2-HaloTag C5* and *AGO2-HaloTag C10* cells (Circled numbers 1-3 in (B)) showing the additional and premature STOP codon in both *AGO2-HaloTag* lines. (F) Abundance of non-HaloTagged *AGO2* mRNA transcript in A549 WT, two UnTagged (*UT C1* and *UT C2*) and two *AGO2-HaloTag* (*AGO2-HaloTag C5* and *AGO2-HaloTag C10*) cells. *AGO2* (non-HaloTagged) mRNA abundance normalised to *B Actin* mRNA abundance and made relative to levels in WT cells. Data represent mean ± SEM of experiments; n = 3 (*p ≤ 0.05; **p ≤ 0.01; ***p ≤ 0.001). (G & H) Western blot of whole-cell lysates from A549 WT, two UnTagged (*UT C1* and *UT C2*) and two *AGO2-HaloTag* (*AGO2-HaloTag C5* and *AGO2-HaloTag C10*) cell lines probed with antibodies against AGO2, HaloTag, and Beta Actin.

Figure 2. Initial Characterisation of AGO2-HaloTag Cells Lines
(A) Doubling time of A549 WT, two UnTagged (*UT C1* and *UT C2*) and two *AGO2-HaloTag* (*AGO2-HaloTag C5* and *AGO2-HaloTag C10*) measured using IncucyteZoom over 108 hours. Data represent mean ± SEM; n = 3 (ns p > 0.05). (B) Representative Western blot of whole-cell lysates from indicated cell lines (harvested during log-phase) probed with antibodies against AGO1, AGO2, AGO3 , AGO4, Vinculin. (C) Representative Western blot of whole-cell lysates from indicated cell lines (harvested during log-phase) probed with antibodies against DDX6, TNRC6A, LIMD1, and Beta Actin.
(D) Densitometry of AGO1/2/3/4 (normalised to loading control (Vinculin)) in indicated cell lines. Data represent mean ± SEM; n = 3 (*p ≤ 0.05; **p ≤ 0.01; ***p ≤ 0.001). (E) Densitometry analysis of Drosha, Exportin 5, Dicer, DGCR8, DDX6 andTNRC6A, (normalised to loading control (Beta Actin or vinculin)) in indicated cell lines. Data represent mean ± SEM; n = 3 (*p ≤ 0.05; **p ≤ 0.01; ***p ≤ 0.001).

Figure 3. Characterising AGO2 interactions, AGO2 localisation and miR-451a levels in AGO2-HaloTag clones.
(A) Endogenous co-immunoprecipitation of AGO2 with Dicer and TNRC6A in WT, UnTagged *C1*, UnTagged *C2, AGO2-HaloTag C5 and AGO2-HaloTag C10* cells. Note the increased AGO2-Dicer and decreased AGO2-TNRC6A co-immunoprecipitation in $AGO2^{HALO}$ cells compared to in WT and UnTagged cells. Histogram shows mean densitometry for TNRC6A IP normalised to AGO2 IP densitometry relative to WT A549 cells. Data represents mean of four independent repeats with * indicating p < 0.05 according to the student's test when comparing UT C2 to AGO2-HaloTag C5 and C10 lines. (B) Immunoblots of nuclear and cytoplasmic fractions from WT. UnTagged *C1*, UnTagged *C2, AGO2-HaloTag C5 and AGO2-HaloTag C10* cells. Whole cell lysate (WCL) from WT A549 was also blotted alongside. Beta tubulin and histone H3 were probed as loading controls for cytoplasmic and nuclear fractions, respectively. (C) *MiR-451a* abundance (normalized to *U6* RNA and made relative to relevant WT) in indicated cell lines measured by RT-qPCR using the $2^{-\Delta\Delta Ct}$ method. Data represent mean ± SEM; n = 2 (*p ≤ 0.05; ***p ≤ 0.001). (D) Pri-miR-451 abundance (normalised to Beta actin mRNA levels) in indicated cell lines measured by RT-qPCR using the standard curve method. Data represent mean ± SEM; n = 2 (*p ≤ 0.05; ***p ≤ 0.001).

1001

1002 **Figure 4. Creation of AGO2 knockout A549, firefly luciferase assays and comparison of N- and C-terminally**
1003 **tagged AGO2.**

1004 (A) Generation of AGO2 knockout A549 cells. Immunoblot of two AGO2$^{-/-}$ clones alongside two control clones
1005 for AGO2 and beta actin as a loading control. (B) Relative Firefly / Renilla Luciferase Activity in indicated cell lines
1006 transfected with reporter plasmids expressing Firefly and Renilla luciferase and a siRNA against Firefly Luciferase
1007 (esi*FFLuc*) or "non-targeting" control (esi*GFP*). The ratio between Firefly and Renilla luciferase activity was
1008 measured 24 h after transfection. Data represent mean ± SEM; n = 3 (ns $p > 0.05$ according to student's unpaired
1009 t-test). (C) Plasmid constructs for expression of untagged AGO2, EGFP-AGO2 and AGO2-EGFP. EGFP-VO is a
1010 control. (D) Relative Firefly / Renilla Luciferase Activity in AGO2$^{-/-}$ A549 transfected with reporter plasmids,
1011 AGO2 plasmids and an siRNA against Firefly Luciferase (esi*FFLuc*) or "non-targeting" control (Scr). The ratio
1012 between Firefly and Renilla luciferase activity was measured 24 h after transfection. Data represent mean ± SEM;
1013 n = 3 (ns $p > 0.05$; ***$p \leq 0.001$ according to student's unpaired t-test). (E) Relative Renilla/Firefly luciferase
1014 activity of a miR-100 targeted (T) reporter relative to a non-targeted (NT) reporter in AGO2$^{-/-}$ A549 transfected
1015 with reporter plasmid, 15 nM miR-100 mimic ad the indicated AGO2 constructs or EGFP-VO. Data represent
1016 mean ± SEM; n = 3 (ns $p > 0.05$; ***$p \leq 0.001$ according to student's unpaired t-test). (F) Immunoblots of nuclear
1017 and cytoplasmic fractions from AGO2$^{-/-}$ A549 transfected with EGFP-VO, AGO2 UT, EGFP-AGO2 or AGO2-EGFP.
1018 Beta tubulin and histone H3 were probed as loading controls for cytoplasmic and nuclear fractions, respectively.
1019 (G) Fluorescence microscopy images for AGO2$^{-/-}$ A549 transfected with EGFP-VO, EGFP-AGO2 or AGO2-EGFP.
1020 Cell nuclei are stained with DAPI and merged images show DAPI and EGFP signal combined. Scale bars indicate
1021 10 µm. (H) UnTagged C1 and *AGO2-HaloTag C10* cells treated with 100 nM HaloTag-TMR ligand visualized using
1022 confocal microscopy.

1023

1024 **Figure 5. Structural Insights of the C-terminal of AGO2 for an Explanation of Impaired Function Upon Halotag**
1025 **Insertion**
1026 (A) Schematic composition of AGO2 showing 7 main domains and motifs. (B) C-terminal residue A859
1027 contributes to miRNA binding (PDB code: 4OLB). Residues shown in stick format and residue type and sequence
1028 number annotated. Dashed lines show inter-atom distances < 5.0 Å. (C) Surface representation of AGO2 (4OLB)
1029 with domains coloured as in (A). Bound miRNA shown in spheres with 5'-3' direction indicated. The approximate
1030 location of the buried C-terminal residue A859 is indicated. (D) Surface representation of AGO2 (4OLB) showing
1031 sites of tryptophan binding and the N-terminal most residue (A22) seen in the electron density. Residues 1-21
1032 were not observed in the data.

1033

1034 **Supplementary Figure 1. STR Profiling for Cell Line Authentication.**
1035 (A) Genetic characteristics of indicated cell lines were investigated by STR profiling using 16 independent PCR-
1036 systems. Cell Line Authentication Test, Eurofins Genomics Europe Applied Genomics GmbH, Anzinger Str. 7 a,
1037 D-85560 Ebersberg
1038 Method: DNA isolation carried out from cell pellet (cell layer). Genetic characteristics were determined by PCR-
1039 single-locus-technology. 16 independent PCR-systems D8S1179, D21S11, D7S820, CSF1PO, D3S1358, TH01,
1040 D13S317, D16S539, D2S1338, AMEL, D5S818, FGA, D19S433, vWA, TPOX and D18S51 were investigated. In
1041 parallel, positive and negative controls were carried out, yielding correct results.
1042 -* no result / weak signal. (B) Genomic DNA sequencing chromatogram traces of the end of the *AGO2* locus in
1043 UnTagged Clone 1 and Clone 2 cells, showing the DNA is not edited. The same region of *AGO2* is shown for WT
1044 A549 for comparison.

Figure 1

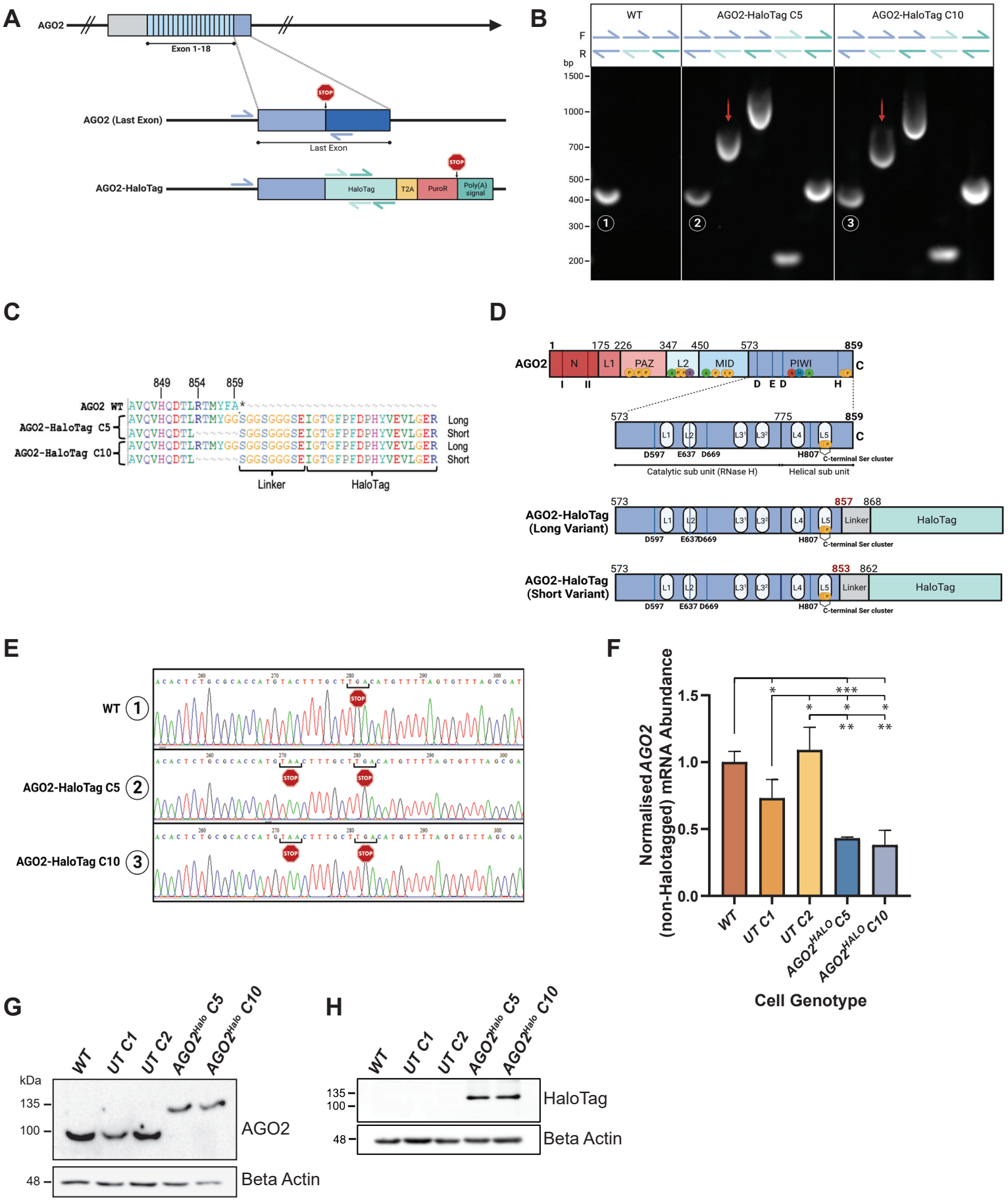
A
AGO2
Exon 1-18
AGO2 (Last Exon)
Last Exon
STOP
AGO2-HaloTag
HaloTag
T2A
PuroR
Poly(A) signal
B
WT
AGO2-HaloTag C5
AGO2-HaloTag C10
F
R
bp
1500
1000
700
500
400
300
200
C
AGO2 WT
AGO2-HaloTag C5
AGO2-HaloTag C10
Long
Short
Linker
HaloTag
D
AGO2
N
L1
PAZ
L2
MID
PIWI
C-terminal Ser cluster
Catalytic sub unit (RNase H)
Helical sub unit
AGO2-HaloTag (Long Variant)
AGO2-HaloTag (Short Variant)
E
WT
AGO2-HaloTag C5
AGO2-HaloTag C10
F
Normalised AGO2 (non-Halotagged) mRNA Abundance
Cell Genotype
WT
UT C1
UT C2
AGO2HALO C5
AGO2HALO C10
G
kDa
135
100
48
AGO2
Beta Actin
H
HaloTag
Beta Actin

Figure 2

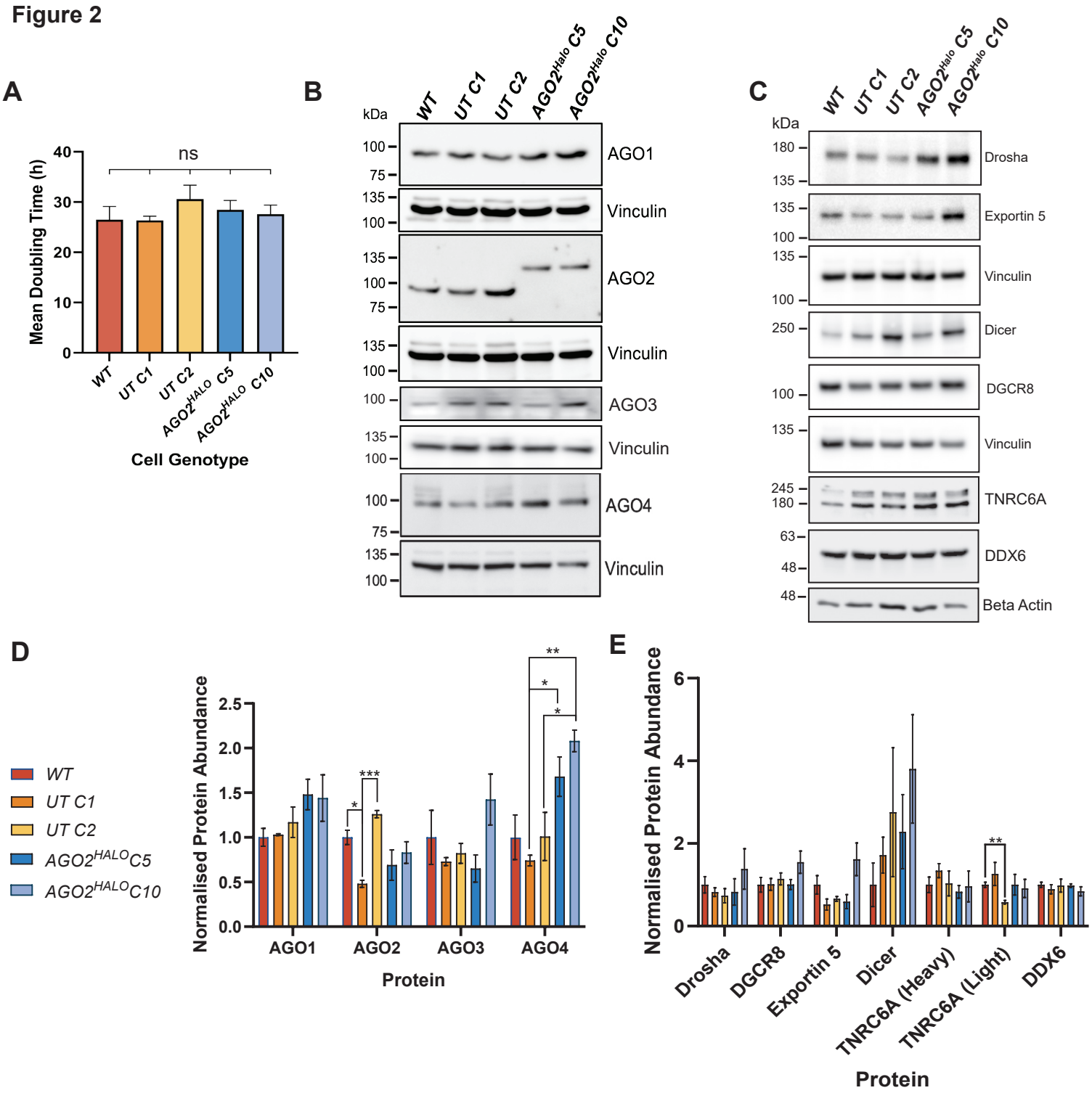
A
Mean Doubling Time (h)
ns
WT
UT C1
UT C2
AGO2HALO C5
AGO2HALO C10
Cell Genotype
B
kDa
WT
UT C1
UT C2
AGO2Halo C5
AGO2Halo C10
AGO1
Vinculin
AGO2
Vinculin
AGO3
Vinculin
AGO4
Vinculin
C
kDa
Drosha
Exportin 5
Vinculin
Dicer
DGCR8
Vinculin
TNRC6A
DDX6
Beta Actin
D
WT
UT C1
UT C2
AGO2HALOC5
AGO2HALOC10
Normalised Protein Abundance
AGO1
AGO2
AGO3
AGO4
Protein
E
Normalised Protein Abundance
Drosha
DGCR8
Exportin 5
Dicer
TNRC6A (Heavy)
TNRC6A (Light)
DDX6
Protein

Figure 3

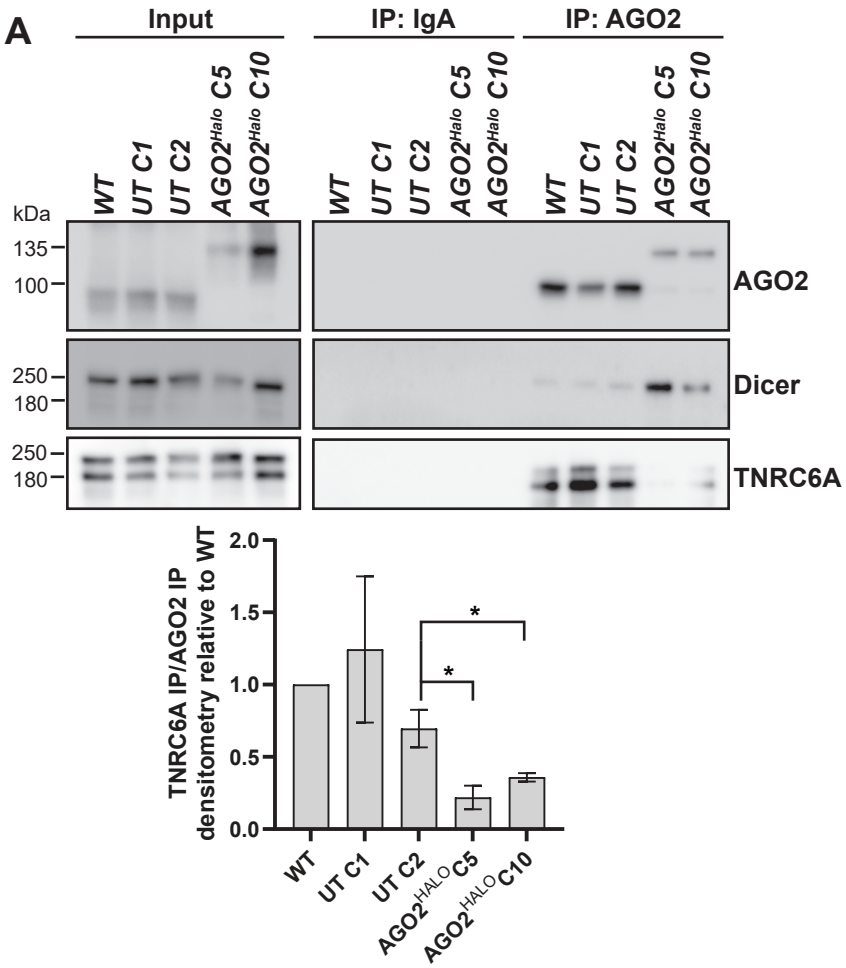
A
Input
IP: IgA
IP: AGO2
WT
UT C1
UT C2
AGO2Halo C5
AGO2Halo C10
kDa
135
100
250
180
AGO2
Dicer
TNRC6A
TNRC6A IP/AGO2 IP densitometry relative to WT
2.0
1.5
1.0
0.5
0.0
*
*
WT
UT C1
UT C2
AGO2HALO C5
AGO2HALO C10

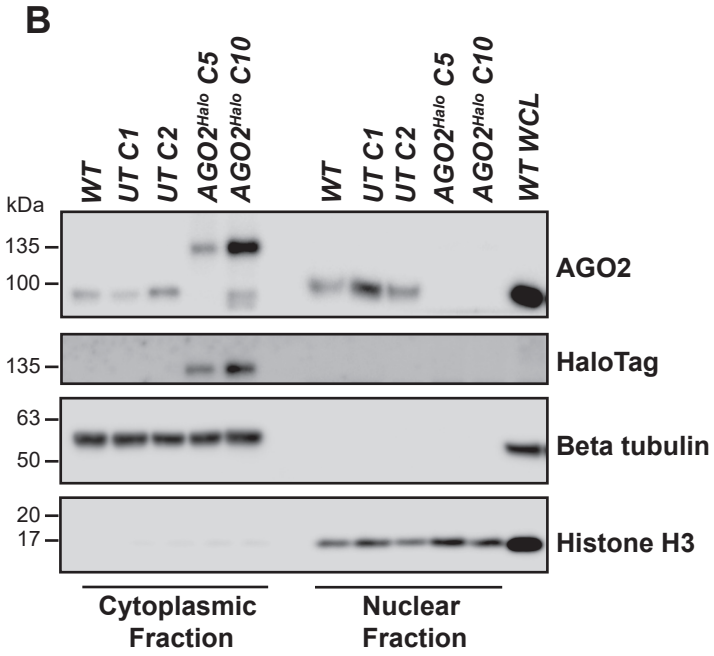
B
WT
UT C1
UT C2
AGO2Halo C5
AGO2Halo C10
WT WCL
kDa
135
100
63
50
20
17
AGO2
HaloTag
Beta tubulin
Histone H3
Cytoplasmic Fraction
Nuclear Fraction

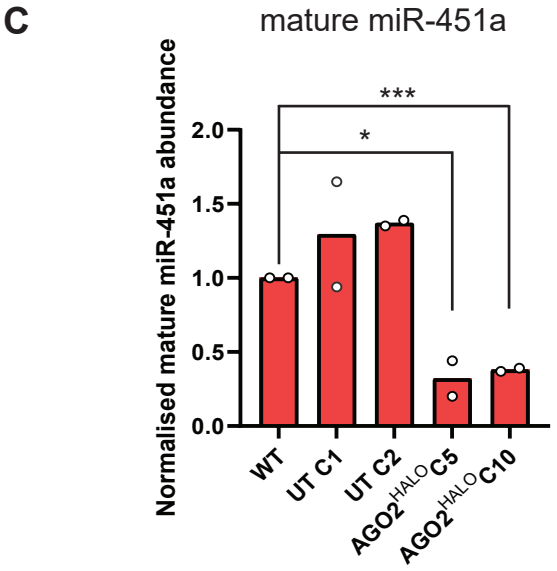
C
mature miR-451a
Normalised mature miR-451a abundance
2.0
1.5
1.0
0.5
0.0
***
*
WT
UT C1
UT C2
AGO2HALO C5
AGO2HALO C10

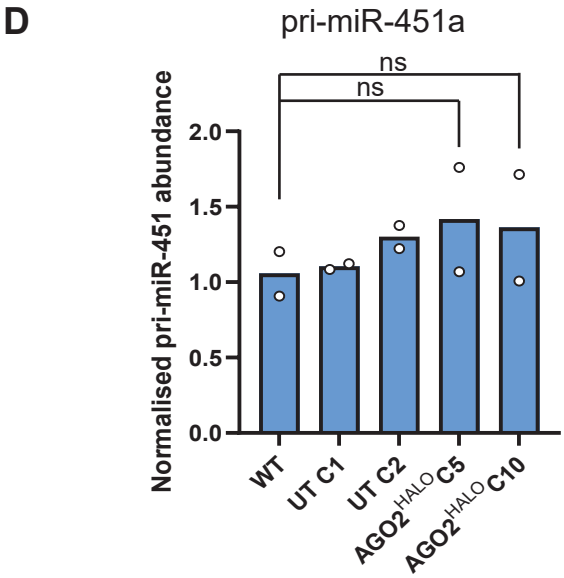
D
pri-miR-451a
Normalised pri-miR-451 abundance
2.0
1.5
1.0
0.5
0.0
ns
ns
WT
UT C1
UT C2
AGO2HALO C5
AGO2HALO C10

Figure 4

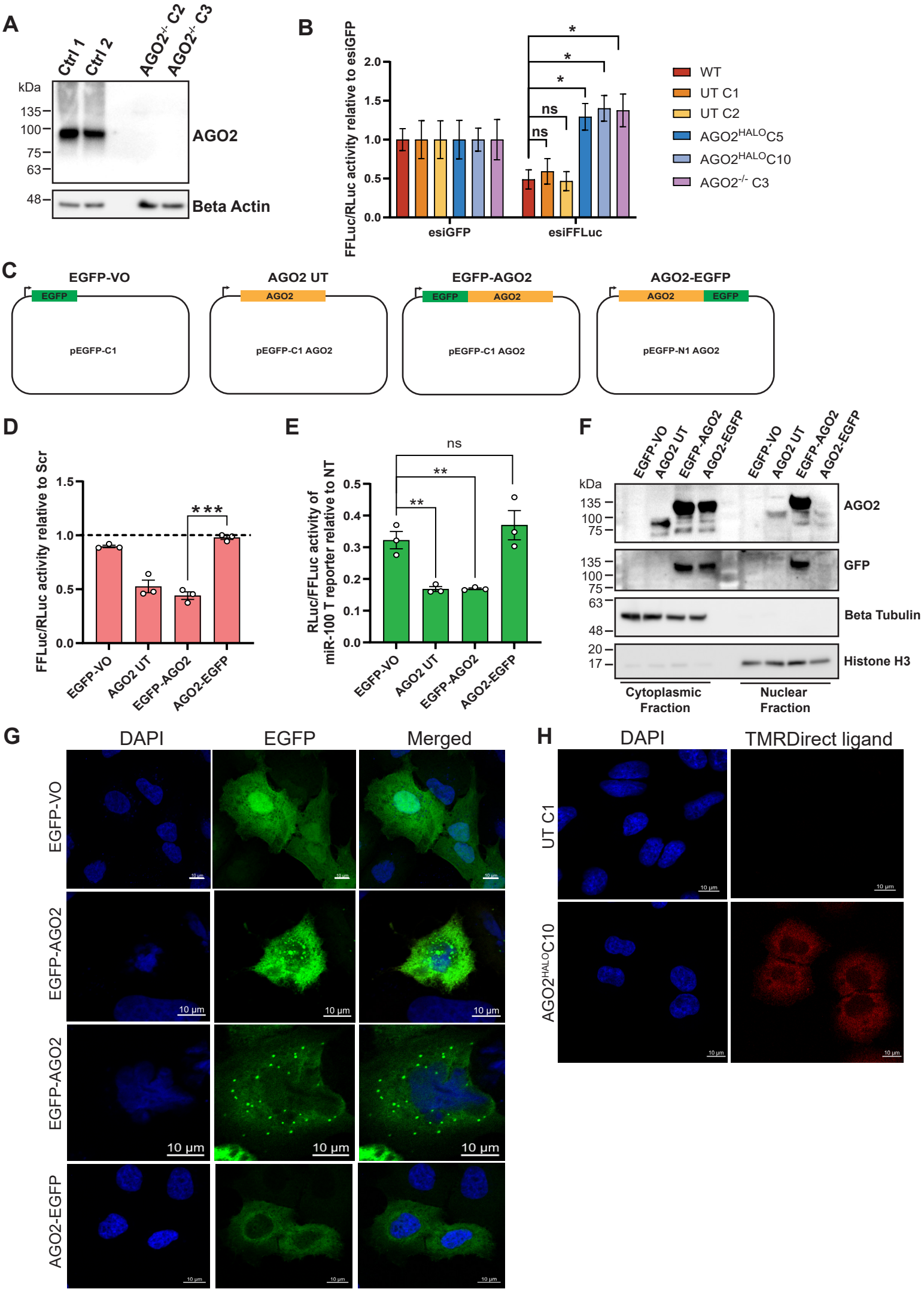
A
Ctrl 1
Ctrl 2
AGO2-/- C2
AGO2-/- C3
kDa
135
100
75
63
48
AGO2
Beta Actin
B
FFLuc/RLuc activity relative to esiGFP
2.0
1.5
1.0
0.5
0.0
*
*
*
ns
ns
esiGFP
esiFFLuc
WT
UT C1
UT C2
AGO2HALOC5
AGO2HALOC10
AGO2-/- C3
C
EGFP-VO
EGFP
pEGFP-C1
AGO2 UT
AGO2
pEGFP-C1 AGO2
EGFP-AGO2
EGFP
AGO2
pEGFP-C1 AGO2
AGO2-EGFP
AGO2
EGFP
pEGFP-N1 AGO2
D
FFLuc/RLuc activity relative to Scr
1.5
1.0
0.5
0.0
***
EGFP-VO
AGO2 UT
EGFP-AGO2
AGO2-EGFP
E
RLuc/FFLuc activity of miR-100 T reporter relative to NT
0.5
0.4
0.3
0.2
0.1
0.0
ns
**
**
EGFP-VO
AGO2 UT
EGFP-AGO2
AGO2-EGFP
F
EGFP-VO
AGO2 UT
EGFP-AGO2
AGO2-EGFP
EGFP-VO
AGO2 UT
EGFP-AGO2
AGO2-EGFP
kDa
135
100
75
AGO2
135
100
75
GFP
63
48
Beta Tubulin
20
17
Histone H3
Cytoplasmic Fraction
Nuclear Fraction
G
DAPI
EGFP
Merged
EGFP-VO
EGFP-AGO2
EGFP-AGO2
AGO2-EGFP
10 µm
H
DAPI
TMRDirect ligand
UT C1
AGO2HALOC10
10 µm

Figure 5

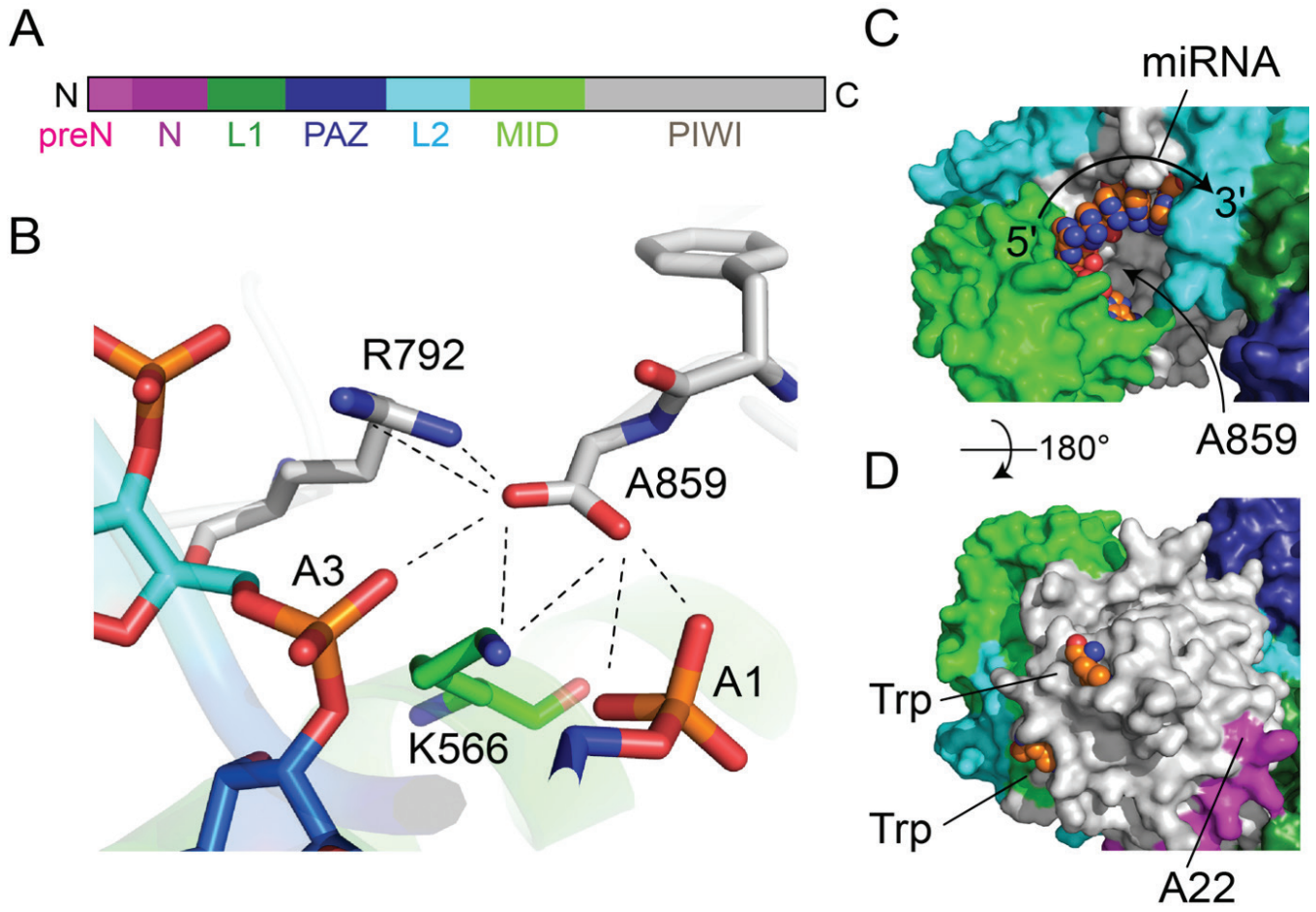
A
N
C
preN
N
L1
PAZ
L2
MID
PIWI
B
R792
A859
A3
A1
K566
C
miRNA
5'
3'
A859
180°
D
Trp
Trp
A22

Supplementary Figure 1

A

	Cell Line			
STR Loci	**A549 WT**	**UnTagged C1**	**AGO2-HaloTag C5**	**AGO2-HaloTag C10**
D8S1179	13,14	13,13	13,14	13,14
D21S11	29,29	29,29	29,29	29,29
D7S820	8,11	8,11	8,11	-*
CSF1PO	10,12	10,12	10,12	-*
D3S1358	16,16	?,?	16,16	16,16
TH01	8,9.3	8,9.3	8,9.3	8,9.3
D13S317	11,11	11,11	11,11	11,11
D16S539	11,12,13	?,12	11,12	11,12
D2S1338	24,24	24,24	24,24	-*
D19S433	13,13	13,13	13,13	13,13
vWA	14,14	14,14	14,14	14,14
TPOX	8,11	8,11	8,11	8,11
D18S51	14,17,18	14,17	14,17	-*
AMEL	X,Y	X,Y	X,X	X,X
D5S818	11,11	11,11	11,11	11,11
FGA	23,23	23,23	23,23	-*

Eurofins Genomics Europe Applied Genomics GmbH, Anzinger Str. 7 a, D-85560 Ebersberg
Cell Line Authentication Test
Method:
DNA isolation was carried out from cell pellets. Genetic characteristics were determined by PCR-single locus technology.
16 Independent PCR-systems D8S1179, D21S11, D7S820, CSF1PO, D3S1358, TH01, D13S317, D16S539, D2S1338, AMEL, D5S818, FGA, D19S433, vWA, TPOX and D18S51 were investigated.
(ASN-0002 core marker s are coloured light blue, ThermoFisher, AmpFISTR(R) Identifiler(R) Plus PCR Amplification kit). In parallel, positive and negative controls were carried out yielding correct results.
-* no result/weak signal.

B
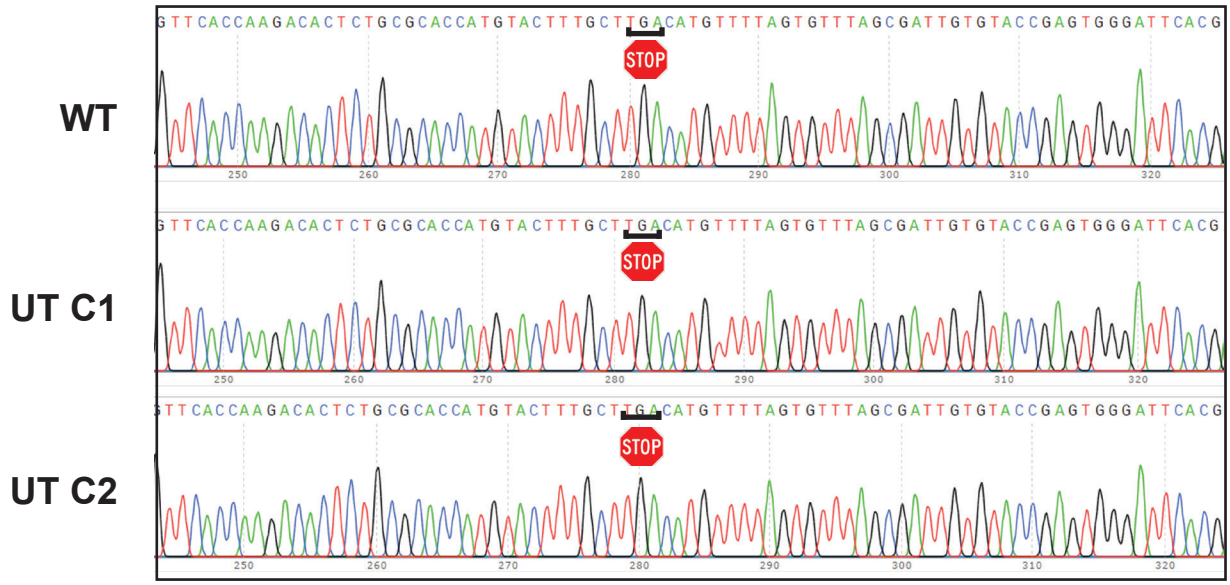
AGO2 locus